11660 *Inorg. Chem.* **2009**, *48*, 11660–11676
DOI: 10.1021/ic901678c

Inorganic Chemistry
Article

Amino Acid Based MOFs: Synthesis, Structure, Single Crystal to Single Crystal Transformation, Magnetic and Related Studies in a Family of Cobalt and Nickel Aminoisophthales

Debajit Sarma,[†] K. V. Ramanujachary,[‡] S. E. Lofland,[§] Travis Magdaleno,[‡] and Srinivasan Natarajan*[,†]

[†]*Framework Solids Laboratory, Solid State and Structural Chemistry Unit, Indian Institute of Science, Bangalore-560012, India,* [‡]*Department of Chemistry and Biochemistry, and* [§]*Department of Physics and Astronomy, Rowan University, 201 Mullica Hill Road, Glassboro, New Jersey 08028*

Received August 24, 2009

Four new 5-aminoisophthalates of cobalt and nickel have been prepared employing hydro/solvothermal methods: $[Co_2(C_8H_5NO_4)_2(C_4H_4N_2)(H_2O)_2]\cdot 3H_2O$ (**I**), $[Ni_2(C_8H_5NO_4)_2(C_4H_4N_2)(H_2O)_2]\cdot 3H_2O$ (**II**), $[Co_2(H_2O)(\mu^3\text{-}OH)_2(C_8H_5NO_4)]$ (**III**), and $[Ni_2(H_2O)(\mu^3\text{-}OH)_2(C_8H_5NO_4)]$ (**IV**). Compounds **I** and **II** are isostructural, having anion-deficient $CdCl_2$ related layers bridged by a pyrazine ligand, giving rise to a bilayer arrangement. Compounds **III** and **IV** have one-dimensional M−O(H)−M chains connected by the 5-aminoisophthalate units forming a three-dimensional structure. The coordinated as well as the lattice water molecules of **I** and **II** could be removed and inserted by simple heating−cooling cycles under the atmospheric conditions. The removal of the coordinated water molecule is accompanied by changes in the coordination environment around the M^{2+} (M = Co, Ni) and color of the samples (purple to blue, Co; green to dark yellow, Ni). This change has been examined by a variety of techniques that include in situ single crystal to single crystal transformation studies and in situ IR and UV−vis spectroscopic studies. Magnetic studies indicate antiferromagnetic behavior in **I** and **II**, a field-induced magnetism in **III**, and a canted antiferromagnetic behavior in **IV**.

Introduction

The inorganic coordination framework materials, more commonly known as metal organic frameworks (MOFs), have undergone important advances over the past decade or so.[1] The interest in these compounds stems from their eminently promising applications for gas storage, sensors, nonlinear optics, luminescence, magnetism, and catalysis.[2] Many MOF compounds possess good structural robustness, flexibility, large pore volumes, and reasonable thermal stability, which sustains the interest in these compounds. The flexibility of the framework has been exploited in studying and controlling the host−guest selectivity as the MOF has both hydrophobic as well as hydrophilic surfaces within the same solid.[3] The generation of the coordinatively unsaturated metal sites by removing bonded (coordinated) guest species promises specific control over the host−guest interactions. The guest molecules, in some cases, have been exchanged for other related guest species, and studies of this nature have also been carried out on single crystals.[4]

*To whom correspondence should be addressed. E-mail: snatarajan@sscu.iisc.ernet.in.

(1) (a) Special Issue on MOF. *Chem. Soc. Rev.* **2009**, *38*, 1213−1504. (b) Mahata, P.; Natarajan, S. *Chem. Soc. Rev.* **2009**, *38*, 2304. (c) Maspoch, D.; Ruiz-Molina, D.; Vaciana, J. *Chem. Soc. Rev.* **2007**, *36*, 770. (d) Rao, C. N. R.; Natarajan, S.; Vaidhyanathan, R. *Angew. Chem., Int. Ed.* **2004**, *43*, 1466. (e) Moulton, B.; Zaworotko, M. J. *Chem. Rev.* **2001**, *101*, 1629.

(2) (a) Mahata, P.; Natarajan, S.; Panissod, P.; Drillon, M. *J. Am. Chem. Soc.* **2009**, *131*, 10140. (b) Morris, R. E.; Wheatley, P. S. *Angew. Chem., Int. Ed.* **2008**, *47*, 4966. (c) Furukawa, H.; Kim, J.; Ockwig, N. W.; O'Keeffe, M.; Yaghi, O. M. *J. Am. Chem. Soc.* **2008**, *130*, 11650. (d) Horike, S.; Dinca, M.; Tamaki, K.; Long, J. R. *J. Am. Chem. Soc.* **2008**, *130*, 5854. (e) Goto, Y.; Sato, H.; Shinkai, S.; Sada, K. *J. Am. Chem. Soc.* **2008**, *130*, 14354. (f) Mahata, P.; Ramya, K. V.; Natarajan, S. *Chem.—Eur. J.* **2008**, *14*, 5839. (g) Maji, T. K.; Matsuda, R.; Kitawaga, S. *Nat. Mater.* **2007**, *6*, 142. (h) Ferey, G.; Mellot-Draznieks, C.; Serre, C.; Millange, F. *Acc. Chem. Res.* **2005**, *38*, 217. (i) Moon, H. R.; Kim, J. H.; Suh, M. P. *Angew. Chem., Int. Ed.* **2005**, *44*, 1261. (j) Kaye, S. S.; Long, J. R. *J. Am. Chem. Soc.* **2005**, *127*, 6506. (k) Kitagawa, S.; Kitaura, R.; Noro, S. *Angew. Chem., Int. Ed.* **2004**, *43*, 2334. (l) Dybtsev, D. N.; Chun, H.; Kim, K. *Angew. Chem., Int. Ed.* **2004**, *43*, 5033. (m) Zhao, X.; Xiao, B.; Fletcher, A. J.; Thoms, K. M.; Bradshaw, D.; Rosseinsky, M. J. *Science* **2004**, *306*, 1012. (n) Rosi, N. L.; Eckert, J.; Eddaoudi, M.; Vodak, D. T.; Kim, J.; O'Keeffe, M.; Yaghi, O. M. *Science* **2003**, *300*, 1127.

(3) (a) Mahata, P.; Ramya, K. V.; Natarajan, S. *Inorg. Chem.* **2009**, *48*, 4942. (b) Ma, S.; Sun, D.; Yuan, D.; Wang, X. S.; Zhou, H. C. *J. Am. Chem. Soc.* **2009**, *131*, 6445. (c) Ma, S.; Sun, D.; Wang, X. S.; Zhou, H. C. *Angew. Chem., Int. Ed.* **2007**, *46*, 2458. (d) Monge, A.; Snejko, N.; Gutiérrez-Puebla, E.; Medina, M.; Cascales, C.; Ruiz-Valero, C.; Iglesias, M.; Gómez-Lor, B. *Chem. Commun.* **2005**, 1291.

(4) (a) Aslani, A.; Morsali, A. *Chem. Commun.* **2008**, 3402. (b) Rather, B.; Zaworotko, M. J. *Chem. Commun.* **2003**, 830. (c) Liu, Y. H.; Tsai, H. L.; Lu, Y. L.; Wen, Y. S.; Wang, J. C.; Li, K. L. *Inorg. Chem.* **2001**, *40*, 6426. (d) Lu, J. Y.; Babb, A. M. *Chem. Commun.* **2002**, 1340. (e) Cussen, E. J.; Claridge, J. B.; Rosseinsky, M. J.; Kepert, C. J. *J. Am. Chem. Soc.* **2002**, *124*, 9574. (f) Biradha, K.; Hongo, Y.; Fujita, M. *Angew. Chem., Int. Ed.* **2000**, *39*, 3843. (g) Li, H.; Eddaoudi, M.; O'Keeffe, M.; Yaghi, O. M. *Nature* **1999**, *402*, 276.

Published on Web 11/25/2009

In addition, the unsaturated metal sites have also been exploited for reversible hydrogen storage studies, especially in compounds containing transition elements.[5]

Many of the reported MOF compounds were synthesized employing benzene polycarboxylic acids.[6] Secondary organic ligands, such as 4,4′-bipyridine, have also been used to control the structure and dimensionality.[7] Studies exploring the relative merits of the reaction time and temperature during the synthesis have also been investigated.[8] A combination of the above studies has resulted in a bewildering variety in the structures for the MOFs. To categorize and catalogue the MOF structures, the node and net based topological description using simple polyhedra and linkers are being employed.[9] This approach helped in understanding the framework structures better and also helped in designing new ones.

Amino carboxylic acids are important in biology and can have zwitterionic behavior. Researchers have employed the amino carboxylic acids for designing new MOF structures.[10] The close structural relationship of the 5-aminoisophthalic acid (AIP) to one of the well-explored benzene tricarboxylic acids (trimesic acid)[11] prompted us to investigate the reactivity of AIP with transition metal ions. A search of the literature revealed that the number of MOFs with 5-AIP[12] was not many in spite of the close resemblance to the trimesic acid. We considered it important to explore the reactivity of 5-AIP with cobalt and nickel by varying a variety of reaction parameters that include the time, the temperature, and the solvent. Our efforts were successful, and we have isolated four new 5-aminoisophthalate phases of cobalt and nickel.

The compounds, $[M_2(C_8H_5NO_4)_2(C_4H_4N_2)(H_2O)_2]\cdot 3H_2O$, M = Co^{2+} (**I**) and Ni^{2+} (**II**) and $[M_2(H_2O)(\mu^3\text{-}OH)_2(C_8H_5NO_4)]$, M = Co^{2+} (**III**) and Ni^{2+} (**IV**), have been prepared and characterized using a variety of techniques. The structures of **I** and **II** are related, having a bilayer two-dimensional arrangement; the structures of **III** and **IV** have three-dimensional structure that possesses one-dimensional M−O(H)−M chains. We have also been able to demonstrate that the coordinated solvent molecules (H_2O) in compounds **I** and **II** can be reversibly exchanged for D_2O. The fully hydrated and dehydrated phases with the coordinatively unsaturated metal sites have also been examined using the single crystal to crystal transformation studies. In this paper, we present the synthesis, structure, single crystal to single crystal transformation studies, adsorption/desorption UV−vis, and magnetic investigations on all of the compounds.

Experimental Section

Synthesis and Initial Characterization. All of the compounds were prepared by employing the hydro/solvothermal method. The various synthesis conditions employed during the present study are given in Table 1. In a typical synthesis for $[Co_2(C_8H_5NO_4)_2(C_4H_4N_2)(H_2O)_2]\cdot 3H_2O$ (**I**), $Co(CH_3COO)_2\cdot 4H_2O$ (0.249 g, 1 mM) was dissolved in 10 mL of water. To this were added 5-aminoisophthalic acid (0.181 g, 1 mM) and pyrazine (0.040 g, 0.5 mM) under continuous stirring. The mixture was homogenized for 30 min at room temperature, transferred and sealed in a 23 mL PTFE lined autoclave, and heated at 75 °C for 3 days under autogenous pressure. The final product contained large quantities of single crystals, which were filtered under vacuum, washed with deionized water, and dried at ambient conditions. A similar procedure was adopted for all of the compounds. In all cases, the products were found to contain large quantities of single crystals along with microcrystalline powders. Thus, purple rod $[Co_2(C_8H_5NO_4)_2(C_4H_4N_2)(H_2O)_2]\cdot 3H_2O$ (**I**) (yield ∼ 74%), light green rod $[Ni_2(C_8H_5NO_4)_2(C_4H_4N_2)(H_2O)_2]\cdot 3H_2O$ (**II**) (yield ∼ 63%), purple block $[Co_2(H_2O)(\mu^3\text{-}OH)_2(C_8H_5NO_4)]$ (**III**) (yield ∼ 65%), and light green block $[Ni_2(H_2O)(\mu^3\text{-}OH)_2(C_8H_5NO_4)]$ (**IV**) (yield ∼ 67%) crystals were obtained (yields are based on Co/Ni). Anal. Calcd for **I**: C, 37.17; H, 3.74; N, 8.67. Found: C,

(5) (a) Xue, D. X.; Zhang, W. X.; Chen, X. M.; Wang, H. Z. *Chem. Commun*. **2008**, 1551. (b) Ye, J.; Liu, Y.; Zhao, Y.; Mu, X.; Zhang, P.; Wang, Y. *CrystEngComm*. **2008**, *10*, 598. (c) Forster, P. M.; Eckert, J.; Heiken, B. D.; Parise, J. B.; Yoon, J. W.; Jhung, S. H.; Chang, J. S.; Cheetham, A. K. *J. Am. Chem. Soc*. **2006**, *128*, 16846. (d) Dietzel, P. D. C.; Morita, Y.; Blom, R.; Fjellvag, H. *Angew. Chem., Int. Ed*. **2005**, *44*, 6354–6358. (e) Suh, M. P.; Ko, J. W.; Choi, H. J. *J. Am. Chem. Soc*. **2002**, *124*, 10976.

(6) (a) Kaye, S. S.; Long, J. R. *J. Am. Chem. Soc*. **2008**, *130*, 806–807. (b) Karabach, Y. Y.; Kirillov, A. M.; Haukka, M.; Sanchiz, J.; Kopylovich, M. N.; Pombeiro, A. J. L. *Cryst. Growth Des*. **2008**, *8*, 4100. (c) Go, Y. B.; Wang, X.; Jacobson, A. J. *Inorg. Chem*. **2007**, *46*, 6594. (d) Wang, X. L.; Qin, C.; Wang, E. B.; Su, Z. M. *Chem.—Eur. J*. **2006**, *12*, 2680. (e) Williams, C. A.; Blake, A. J.; Hubberstey, P.; Schroder, M. *Chem. Commun*. **2005**, *43*, 5435. (f) Ganesan, S. V.; Natarajan, S. *J. Chem. Sci*. **2004**, *116*, 65. (g) Gomez-Lor, B.; Gutierrez, P. E.; Iglesias, M.; Monge, M. A.; Ruiz-Valero, C.; Snejko, N. *Inorg. Chem*. **2002**, *41*, 2429. (h) Eddaoudi, M.; Moler, D. B.; Li, H.; Chen, B.; Reineke, T. M.; O'Keeffe, M.; Yaghi, O. M. *Acc. Chem. Res*. **2001**, *34*, 319. (i) Eddaoudi, M.; Li, H.; Yaghi, O. M. *J. Am. Chem. Soc*. **2000**, *122*, 1391. (j) Reineke, T. M.; Eddaoudi, M.; O'Keeffe, M.; Yaghi, O. M. *Angew. Chem., Int. Ed*. **1999**, *38*, 2590. (k) Li, H.; Eddaoudi, M.; O'Keeffe, M.; Yaghi, O. M. *Nature* **1999**, *402*, 276. (l) Li, H.; Eddaoudi, M.; Groy, T. L.; Yaghi, O. M. *J. Am. Chem. Soc*. **1998**, *120*, 8571.

(7) (a) Jiang, Y.; Huang, J.; Kasumaj, B.; Jeschke, G.; Hunger, M.; Mallat, T.; Baiker, A. *J. Am. Chem. Soc*. **2009**, *131*, 2058. (b) Li, Y.; Xie, L.; Liu, Y.; Yang, R.; Li, X. *Inorg. Chem*. **2008**, *47*, 10372. (c) Pichon, A.; Fierro, C. M.; Nieuwenhuyzen, M.; James, S. L. *CrystEngComm*. **2007**, *9*, 449. (d) Maji, T. K.; Ohba, M.; Kitagawa, S. *Inorg. Chem*. **2005**, *44*, 9225. (e) Gómez-Lor, B.; Gutiérrez-Puebla, E.; Iglesias, M.; Monge, M. A.; Ruiz-Valero, C.; Snejko, N. *Chem. Mater*. **2005**, *17*, 2568. (f) Biradha, K.; Fujita, M. *Chem. Commun*. **2001**, 15. (g) Noro, S.; Kitagawa, S.; Kondo, M.; Seki, K. *Angew. Chem., Int. Ed*. **2000**, *39*, 2082. (h) Kondo, M.; Yoshitomi, T.; Seki, K.; Matsuzaka, H.; Kitagawa, S. *Angew. Chem., Int. Ed*. **1997**, *36*, 1725.

(8) (a) Mahata, P.; Prabu, M.; Natarajan, S. *Inorg. Chem*. **2008**, *47*, 8451. (b) Zhang, J.; Bu, X. *Chem. Commun*. **2008**, 444. (c) Cheetham, A. K.; Rao, C. N. R.; Feller, R. K. *Chem. Commun*. **2006**, 4780. (d) Wang, X. L.; Qin, C.; Wang, E. B.; Li, Y. G.; Su, Z. M.; Xu, L.; Carlucci, L. *Angew. Chem., Int. Ed*. **2005**, *44*, 5824. (e) Tong, M. L.; Kitagawa, S.; Chang, H. C.; Ohba, M. *Chem. Commun*. **2004**, 418.

(9) (a) Wells, A. F. *Three-Diemsional Nats and Polyhedra*; John Wiley and Sons: New York, 1977. (b) O'Keefe, M.; Hyde, B. G. *Philos. Trans*. **1980**, *295*, 553.

(10) (a) Vaidhyanathan, R.; Bradshaw, D.; Rebilly, J.; Barrio, J. P.; Gould, J. A.; Berry, N. G.; Rosseinsky, M. J. *Angew. Chem., Int. Ed*. **2006**, *45*, 1. (b) Anokhina, E. V.; Go, Y. B.; Lee, Y.; Vogt, T.; Jacobson, A. J. *J. Am. Chem. Soc*. **2006**, *128*, 9957. (c) Chen, L.; Bu, X. *Chem. Mater*. **2006**, *18*, 1857. (d) Mercier, N.; Riou, A. *Chem. Commun*. **2004**, 844. (e) Wang, R.; Liu, H.; Carducci, M. D.; Jin, T.; Zheng, C.; Zheng, Z. *Inorg. Chem*. **2001**, *40*, 2743.

(11) (a) Volkringer, C.; Meddouri, M.; Loiseau, T.; Guillou, N.; Marrot, J.; Ferey, G.; Haouas, M.; Taulelle, F.; Audebrand, N.; Latroche, M. *Inorg. Chem*. **2008**, *47*, 11892. (b) Li, Z.; Zhu, G.; Guo, X.; Zhao, X.; Jin, Z.; Qiu, S. *Inorg. Chem*. **2007**, *46*, 5174. (c) Guo, X.; Zhu, G.; Li, Z.; Chen, Y.; Li, X.; Qiu, S. *Inorg. Chem*. **2007**, *46*, 4065. (d) Pascu, M.; Lloret, F.; Avarvari, N.; Julve, M.; Andruh, M. *Inorg. Chem*. **2004**, *43*, 5189. (e) Kim, J.; Chen, B.; Reineke, T. M.; Li, H.; Eddaoudi, M.; Moler, D. B.; O'Keeffe, M.; Yaghi, O. M. *J. Am. Chem. Soc*. **2001**, *123*, 8239. (f) Gutschke, S. O. H.; Molinier, M.; Powell, A. K.; Winpenny, R. E. P.; Wood, P. T. *Chem. Commun*. **1996**, 823. (g) Chui, S. S. Y.; Lo, M. F.; Charmant, J. P. H.; Orpen, A. G.; Williams, I. D. *Science* **1999**, *283*, 1148.

(12) (a) Furukawa, H.; Kim, J.; Ockwig, N. W.; O'Keeffe, M.; Yaghi, O. M. *J. Am. Chem. Soc*. **2008**, *130*, 11650. (b) Huang, Y.; Yan, B.; Shao, M. *Solid State Sci*. **2008**, *10*, 90. (c) Huang, J. Y.; Liang, H. *J. Mol. Struct*. **2008**, *876*, 162. (d) Kongshaug, K. O.; Fjellvag, H. *Polyhedron* **2007**, *26*, 5113. (e) Zhang, K. L.; Qiao, N.; Gao, H. Y.; Ming Zhang, F. Z. *Polyhedron* **2007**, *26*, 2461. (f) Murugavel, R.; Kumar, P.; Walawalkar, M. G.; Mathialagan, R. *Inorg. Chem*. **2007**, *46*, 6828. (g) McManus, G. J.; Wang, Z.; Beauchamp, D. A.; Zaworotko, M. J. *Chem. Commun*. **2007**, 5212. (h) Tao, J.; Yin, X.; Jiang, Y. B.; Huang, R. B.; Zheng, L. S. *Inorg. Chem. Commun*. **2003**, 1171. (i) Wu, C. D.; Lu, C. Z.; Zhuang, H. H.; Huang, J. S. *Z. Anorg. Allg. Chem*. **2002**, *628*, 1935.

Table 1. Synthesis Conditions Employed for Compounds **I**−**IV**

synthesis condition				composition
mole ratio	temp (°C)	time (h)	yields[a] (%)	product
$Co(CH_3COO)_2 \cdot 4H_2O$ + AIP + 0.5 pyrazine + 556 H_2O	75	72	74	$[Co_2(C_8H_5NO_4)_2(C_4H_4N_2)(H_2O)_2] \cdot 3H_2O$ (**I**)
$Ni(CH_3COO)_2 \cdot 4H_2O$ + AIP + 0.5 pyrazine + 556 H_2O	75	72	63	$[Ni_2(C_8H_5NO_4)_2(C_4H_4N_2)(H_2O)_2] \cdot 3H_2O$ (**II**)
$Co(CH_3COO)_2 \cdot 4H_2O$ + 0.5 AIP + 4,4′-bipyridine + 278 H_2O + 156 CH_3OH	200	72	65	$[Co_2(H_2O)(\mu^3\text{-}OH)_2(C_8H_5NO_4)]$ (**III**)
$Ni(CH_3COO)_2 \cdot 4H_2O$ + 0.5 AIP + 4,4′-bipyridine + 278 H_2O + 156 CH_3OH	200	72	67	$[Ni_2(H_2O)(\mu^3\text{-}OH)_2(C_8H_5NO_4)]$ (**IV**)

[a] Yields are based on the metal (Co/Ni).

Table 2. Crystal Data and Structure Refinement Parameters for Compounds **I**−**IV**[a]

	$[Co_2(C_8H_5NO_4)_2(C_4H_4N_2)(H_2O)_2] \cdot 3H_2O$ (**I**)	$[Co_2(C_8H_5NO_4)_2(C_4H_4N_2)]$ (**Ia**)	$[Ni_2(C_8H_5NO_4)_2(C_4H_4N_2)(H_2O)_2] \cdot 3H_2O$ (**II**)	$[Ni_2(C_8H_5NO_4)_2(C_4H_4N_2)]$ (**IIa**)	$[Co_2(H_2O)(\mu^3\text{-}OH)_2(C_8H_5NO_4)]$ (**III**)	$[Ni_2(H_2O)(\mu^3\text{-}OH)_2(C_8H_5NO_4)]$ (**IV**)
empirical formula	$C_{20}H_{24}N_4O_{13}Co_2$	$C_{10}H_7N_2O_4Co$	$C_{20}H_{24}N_4O_{13}Ni_2$	$C_{10}H_7N_2O_4Ni$	$C_8H_9NO_7Co_2$	$C_8H_9NO_7Ni_2$
formula weight	646.26	278.11	645.76	277.89	349.02	348.58
crystal system	triclinic	monoclinic	triclinic	monoclinic	monoclinic	monoclinic
space group	$P\bar{1}$ (no. 2)	$C2/c$ (no. 15)	$P\bar{1}$ (no. 2)	$C2/c$ (no. 15)	$P2_1/c$ (no. 14)	$P2_1/c$ (no. 14)
a/Å	7.833(1)	21.134(1)	7.820(1)	21.096(8)	5.264(1)	5.181(1)
b/Å	11.102(1)	7.740(1)	11.190(1)	7.845(3)	11.727(3)	11.569(1)
c/Å	14.855(2)	15.908 (1)	14.717(2)	15.635(6)	16.330(4)	16.596(1)
α/°	73.002(2)	90	72.772(2)	90	90.0	90.0
β/°	77.365(2)	117.625(2)	77.226(2)	116.381(16)	93.399(4)	92.362(2)
γ/°	71.665(2)	90	71.839(2)	90	90.0	90.0
volume/Å^3	1161.2(2)	2305.58(14)	1156.9(2)	2318.2(15)	1006.3(4)	993.83(4)
Z	2	8	2	8	4	4
T/K	293(2)	398(2)	293(2)	398(2)	293(2)	293(2)
ρ_{calc} (g cm^{-3})	1.837	1.602	1.843	1.592	2.290	2.316
μ (mm^{-1})	1.509	1.492	1.709	1.677	3.324	3.817
θ range (deg)	1.45 to 27.87	2.18 to 26.17	1.46 to 28.07	2.16 to 22.77	2.14 to 28.05	2.15 to 23.32
λ (Mo Kα) (Å)	0.71073	0.71073	0.71073	0.71073	0.71073	0.71073
reflection collected	13515	13899	13538	8692	8494	6709
unique reflections	5326	2300	5375	1500	2369	1432
number of parameters	392	182	392	182	179	179
R_{int}	0.0472	0.0345	0.0352	0.0713	0.0227	0.0304
R indices [$I > 2\sigma(I)$]	$R1$ = 0.0623, $wR2$ = 0.1294	$R1$ = 0.0269, $wR2$ = 0.0595	$R1$ = 0.0598, $wR2$ = 0.1521	$R1$ = 0.0304, $wR2$ = 0.0645	$R1$ = 0.0372, $wR2$ = 0.0912	$R1$ = 0.0267, $wR2$ = 0.0622
R indices (all data)	$R1$ = 0.0900, $wR2$ = 0.1412	$R1$ = 0.0488, $wR2$ = 0.0701	$R1$ = 0.0758, $wR2$ = 0.1626	$R1$ = 0.0579, $wR2$ = 0.0771	$R1$ = 0.0466, $wR2$ = 0.0967	$R1$ =0.0401, $wR2$ = 0.0699

[a] $R_1 = \Sigma||F_o| - |F_c||/\Sigma|F_o|$; $wR2 = \{\Sigma[w(F_o^2 - F_c^2)]/\Sigma[w(F_o^2)^2]\}^{1/2}$; $w = 1/[\rho^2(F_o)^2 + (aP)^2 + bP]$; $P = [\max(F_o,O) + 2(F_c)^2]/3$, where a = 0.0534 and b = 2.2742 for **I**, a = 0.0279 and b = 2.6214 for **Ia**, a = 0.0932 and b = 1.3712 for **II**, a = 0.0357 and b = 0.0000 for **IIa**, a = 0.0440 and b = 3.1512 for **III**, a = 0.0299 and b = 2.1383 for **IV**.

38.11; H, 3.46; N, 8.85. Anal. Calcd for **II**: C, 37.20; H, 3.75; N, 8.68. Found: C, 37.91; H, 3.96; N, 8.43. Anal. Calcd for **III**: C, 27.53; H, 2.60; N, 4.01. Found: C, 27.66; H, 2.73; N, 3.97. Anal. Calcd for **IV**: C, 27.57; H, 2.60; N, 4.02. Found: C, 27.79; H, 2.35; N, 4.14.

Initial characterizations were carried out by elemental analysis, powder X-ray diffraction (XRD), thermogravimetric analysis, and IR and UV−vis spectroscopic studies. Powder X-ray diffraction (XRD) patterns were recorded in the 2θ range of 5−50° using Cu Kα radiation (Philips X'pert) (see Supporting Information, Figures S1−S4). IR spectra for all of the compounds were recorded as KBr pellets (Perkin-Elmer, SPECTRUM 1000). The mid-IR spectroscopic studies did not reveal bands corresponding to the metal−ligand vibrational modes, as they appear less than the 400 cm^{-1} range. The spectra exhibited typical peaks corresponding to the water molecule, the amino group, the carboxylate groups, etc. for all of the compounds with little variations in their respective bands (see Supporting Information, Figure S5). Important observed IR bands are γ_{as}(O−H) = 3401−3636 cm^{-1}, γ_s(N−H) = 3154−3348 cm^{-1}, γ_s(C−H)$_{aromatic}$ = 2916−2923 cm^{-1}, γ_s(C═O) = 1617−1626 cm^{-1}, $\delta(H_2O)$ = 1535−1575 cm^{-1}, δ(COO) = 1371−1390 cm^{-1}, γ_s(C−C)$_{skeletal}$ = 1010−1098 cm^{-1}, δ(CN)$_{skeletal}$ = 956−964 cm^{-1}, and δ(CH$_{aromatic}$)$_{outofplane}$ = 780−788 cm^{-1} (see Table S1).

Single Crystal Structure Determination. A suitable single crystal of each compound was carefully selected under a polarizing microscope and glued to a thin glass fiber. The single crystal data were collected on a Bruker AXS smart Apex CCD diffractometer at 293(2) K. The X-ray generator was operated at 50 kV and 35 mA using Mo Kα (λ = 0.71073 Å) radiation. Data were collected with ω scan width of 0.3°. A total of 606 frames were collected in three different setting of φ (0, 90, 180°) keeping the sample-to-detector distance fixed at 6.03 cm and the detector position (2θ) fixed at −25°. The data were reduced using SAINTPLUS,[13] and an empirical absorption correction was applied using the SADABS program.[14] The structure was solved and refined using SHELXL97[15]

(13) *SMART*, version 5.628; *SAINT*, version 6.45a; *XPREP*; *SHELXTL*; Bruker AXS Inc.: Madison, WI, **2004**.

(14) Sheldrick, G. M. *Siemens Area Correction Absorption Correction Program*; University of Göttingen: Göttingen, Germany, **1994**.

(15) Sheldrick, G. M. *SHELXL-97*, Program for Crystal Structure Solution and Refinement; University of Göttingen: Göttingen, Germany, 1997.

Table 3. Selected Observed Bond Distances in Compounds **I**–**IV**[a]

bond	distances (Å)	bond	distances (Å)	bond	distances (Å)
		$[Co_2(C_8H_5NO_4)_2(C_4H_4N_2)(H_2O)_2]\cdot 3H_2O$ (**I**)			
Co(1)–O(1)	1.977(3)	Co(1)–N(2)	2.210(4)	Co(2)–N(3)	2.099(4)
Co(1)–N(1)	2.092(4)	Co(1)–O(4)	2.240(3)	Co(2)–N(4)#2	2.149(4)
Co(1)–O(2)	2.099(3)	Co(2)–O(5)#1	1.982(3)	Co(2)–O(7)	2.239(4)
Co(1)–O(3)	2.164(4)	Co(2)–O(6)	2.071(3)	Co(2)–O(8)	2.312(3)
		$[Co_2(C_8H_5NO_4)_2(C_4H_4N_2)]$ (**Ia**)			
Co(1)–O(1)	1.939(2)	Co(1)–N(1)	2.085(2)	Co(1)–O(4)#1	2.348(2)
Co(1)–O(2)#1	2.006(2)	Co(1)–N(2)#2	2.094(2)		
		$[Ni_2(C_8H_5NO_4)_2(C_4H_4N_2)(H_2O)_2]\cdot 3H_2O$ (**II**)			
Ni1–O(1)	1.993(3)	Ni1–O(4)	2.131(3)	Ni2–N(4)#2	2.098(4)
Ni1–N(1)	2.040(4)	Ni1–N(2)	2.153(4)	Ni2–O(6)	2.102(3)
Ni1–O(2)	2.110(3)	Ni2–O(5)#1	2.021(3)	Ni2–O(7)	2.134(4)
Ni1–O(3)	2.126(3)	Ni2–N(3)	2.064(4)	Ni2–O(8)	2.161(3)
		$[Ni_2(C_8H_5NO_4)_2(C_4H_4N_2)]$ (**IIa**)			
Ni(1)–O(1)	1.952(3)	Ni(1)–N(1)	2.057(3)	Ni(1)–O(4)#2	2.119(3)
Ni(1)–N(2)#1	2.046(4)	Ni(1)–O(2)#2	2.076(3)		
		$[Co_2(H_2O)(\mu^3\text{-}OH)_2(C_8H_5NO_4)]$ (**III**)			
Co(1)–O(2)#1	2.052(3)	Co(1)–O(4)	2.122(3)	Co(2)–O(6)	2.054(3)
Co(1)–O(1)	2.092(3)	Co(1)–O(2)	2.164(3)	Co(2)–O(2)	2.119(3)
Co(1)–O(1)#2	2.095(3)	Co(2)–O(1)	2.039(3)	Co(2)–N(1)	2.212(3)
Co(1)–O(3)	2.107(3)	Co(2)–O(5)	2.049(3)	Co(2)–O(7)	2.358(6)
		$[Ni_2(H_2O)(\mu^3\text{-}OH)_2(C_8H_5NO_4)]$ (**IV**)			
Ni(1)–O(1)	2.051(3)	Ni(1)–O(4)	2.084(3)	Ni(2)–O(6)	2.038(3)
Ni(1)–O(2)#1	2.052(4)	Ni(1)–O(2)	2.106(3)	Ni(2)–O(2)	2.069(4)
Ni(1)–O(3)	2.060(3)	Ni(2)–O(1)	2.022(3)	Ni(2)–N(1)	2.150(4)
Ni(1)–O(1)#2	2.061(3)	Ni(2)–O(5)	2.032(3)	Ni(2)–O(7)	2.247(4)

[a] Symmetry transformations used to generate equivalent atoms. For **I**: #1 $x-1,y-1,z+1$; #2 $x-1,y,z$. For **Ia**: # $x,-y+1,z-1/2$; #2 $x,-y+2,z-1/2$. For **II**: #1 $x-1,y-1,z+1$; #2 $x-1,y,z$. For **IIa**: #1 $x,-y+2,z-1/2$; #2 $x,-y+1,z-1/2$. For **III**: #1 $-x+1,-y+1,-z+1$; #2 $-x,-y+1,-z+1$. For **IV**: #1 $-x+1,-y+1,-z+1$; #2 $-x,-y+1,-z+1$.

present in the WinGx suite of programs (version 1.63.04a).[16] All hydrogen positions were initially located in the difference Fourier maps, and for the final refinement, the hydrogen atoms were placed in geometrically ideal positions and refined in the riding mode. Restraints for the bond distances were used during the refinement for keeping the hydrogen atoms bonded to the water molecules. Final refinement included atomic positions for all of the atoms, anisotropic thermal parameters for all of the non-hydrogen atoms, and isotropic thermal parameters for all hydrogen atoms. Full-matrix least-squares refinement against $|F^2|$ was carried out using the WinGx package of programs.[16] Details of the structure solution and final refinements for the compounds are given in Table 2. CCDC 742136-742143 contains the crystallographic data (compounds **I**–**IV**) for this paper. These data can be obtained free of charge from The Cambridge Crystallographic Data Center (CCDC) via www.ccdc.cam.ac.uk/data_request/cif.

Results and Discussion

Structure of $[M_2(C_8H_5NO_4)_2(C_4H_4N_2)(H_2O)_2]\cdot 3H_2O$, M = Co^{2+} (I) and Ni^{2+} (II). The compounds $[Co_2(C_8H_5NO_4)_2(C_4H_4N_2)(H_2O)_2]\cdot 3H_2O$ (**I**) and $[Ni_2(C_8H_5NO_4)_2(C_4H_4N_2)(H_2O)_2]\cdot 3H_2O$ (**II**) are isostructural, and the asymmetric unit consists of two crystallographically independent M^{2+} ions (M = Co and Ni), two 5-aminoisophthalate (AIP) anions, one pyrazine molecule, and five water molecules. The metal ions have distorted octahedral coordination formed by three carboxylate oxygens, one nitrogen from the amino group of the AIP anion, one nitrogen from the pyrazine ligand, and a coordinated water molecule. The M–O bond distances are in the range of 1.977(3)–2.312(3) Å for Co (av. 2.136 Å) and 1.994(3)–2.161(3) Å for Ni (av. 2.098 Å); the M–N bond distances are in the range of 2.092(4)–2.210(4) Å for Co (av. 2.138 Å) and 2.042(4)–2.155(4) Å for Ni (av. 2.091 Å). The O/N–M–O/N bond angles are in the range of 60.26(11)–177.72(15)° for Co and 61.93(11)–175.84(13)° for Ni. The selected bond distances are listed in Table 3.

The structure consists of a linkage between the octahedral metal centers, the AIP anions, and the pyrazine ligands. Each AIP anion is bonded with three different metal centers by one monocoordinated carboxylate, one chelating carboxylate, and one amino group, and each metal center connects with three different AIP anions (see Supporting Information, Figure S6). This connectivity between the AIP and the metal centers results in a two-dimensional layer that closely resembles the 3^6 topology (Figure 1a). The organic ligand, pyrazine, connects two alternate adjacent layers, forming a bilayer arrangement. The bonded water molecules project into the bilayer spaces. The free lattice water molecules also occupy spaces within the bilayers (Figure 1b). Similar bilayers connected by bipyridine were reported recently.[17]

(16) Farrugia, J. L. *J. Appl. Crystallogr.* **1999**, *32*, 837.

(17) Zeng, M. H.; Hu, S.; Chen, Q.; Xie, G.; Shuai, Q.; Gao, S. L.; Tang, L. Y. *Inorg. Chem.* **2009**, *48*, 7070.

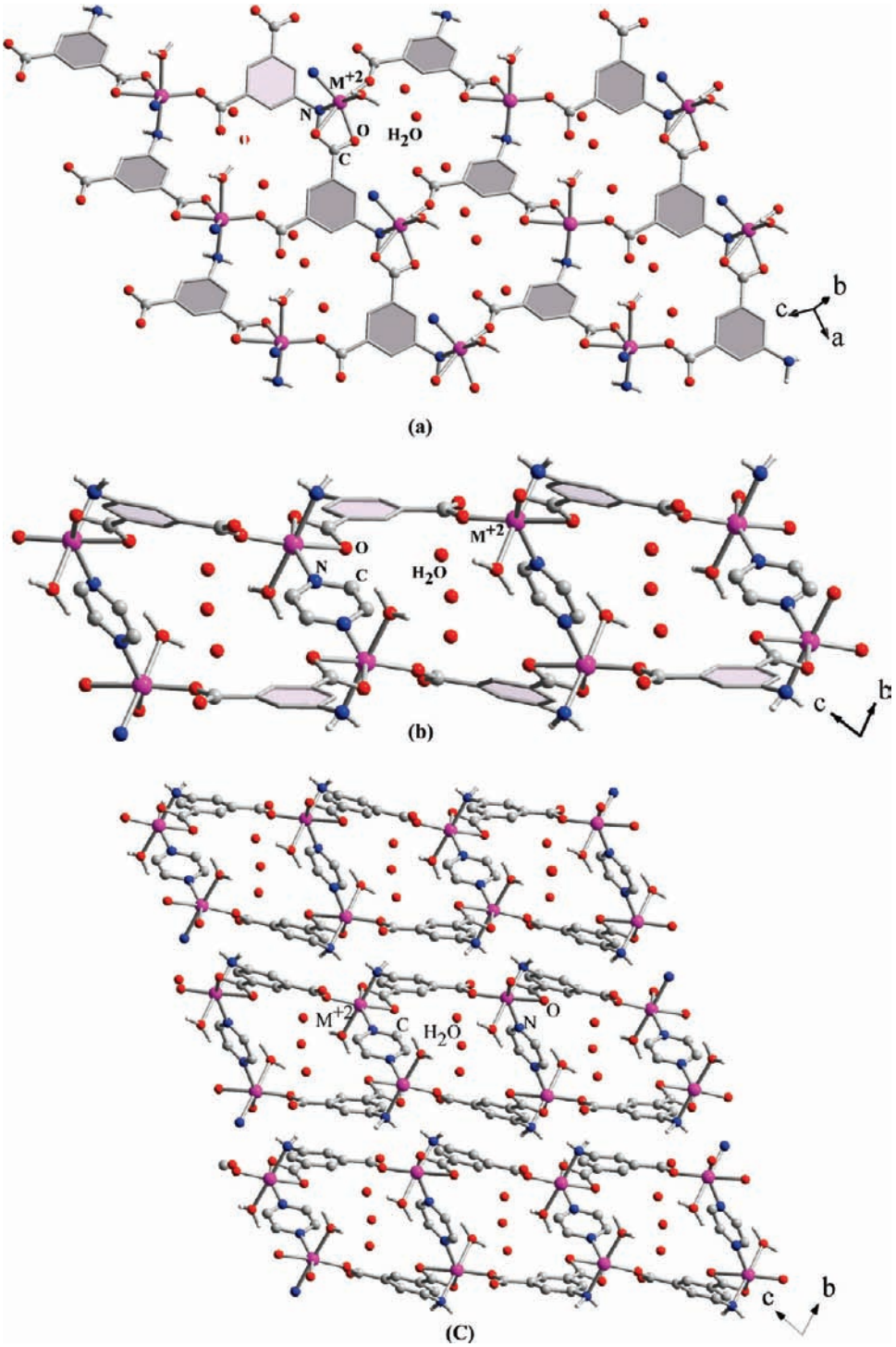

Figure 1. (a) View of the two-dimensional layer in $[Co_2(C_8H_5NO_4)_2(C_4H_4N_2)(H_2O)_2]\cdot 3H_2O$ (**I**) and $[Ni_2(C_8H_5NO_4)_2(C_4H_4N_2)(H_2O)_2]\cdot 3H_2O$ (**II**). (b) Connectivity between the layers by pyrazine ligand in **I** and **II** forming a bilayer arrangement. (c) View of the arrangement of bilayers in **I** and **II**.

The close proximity of the water molecules, coordinated [O(3) and O(7)] and lattice water [O(100), O(200), and O(300)] gives rise to interesting hydrogen bond interactions of the O−H···O type. In addition, the water molecules also interact with the framework oxygens. The important O−H···O interactions with O···O contact distances are in the range of 2.724(8)−3.016(6) Å for $[Co_2(C_8H_5NO_4)_2(C_4H_4N_2)(H_2O)_2]\cdot 3H_2O$ (**I**) and 2.735(7)−3.111(8) Å for $[Ni_2(C_8H_5NO_4)_2(C_4H_4N_2)(H_2O)_2]\cdot 3H_2O$ (**II**), and the O−H···O bond angles are in the range of 146−168° (**I**) and 160−174° (**II**). This suggests that the hydrogen bond interactions are relatively strong.[18] Since we have the amino group bonded to the metal centers, we also observe N−H···O type hydrogen bonds in both compounds. The N···O distances of 2.944(5)−3.153(6) Å (**I**) and 2.932(5)−3.200(6) Å (**II**) and N−H···O bond angles of 141−155° (**I**) and 141−169°

(18) Scheiner, S. *Hydrogen Bonding: A Theoritical Perspectivite*; Oxford University Press: New York, 1997.

Table 4. Important H-Bonding Interactions Observed in Compounds **I**–**IV**[a]

D−H···A	D−H (Å)	H···A (Å)	D···A (Å)	D−H···A (°)
		$[Co_2(C_8H_5NO_4)_2(C_4H_4N_2)(H_2O)_2]\cdot 3H_2O$ (**I**)		
N(2)−H(21)···O(9) #a	1.00(7)	2.28(7)	3.153(6)	145
N(2)−H(22)···O(6) #b	0.68(4)	2.31(5)	2.975(5)	168
O(3)−H(31)···O(4) #c	0.94(5)	1.95(5)	2.879(5)	168
O(3)−H(32)···O(100) #d	0.95(6)	2.06(6)	2.970(7)	162
N(4)−H(41)···O(10) #e	0.88(7)	2.33(7)	3.067(6)	141
N(4)−H(42)···O(2) #b	0.80(6)	2.16(6)	2.944(5)	169
O(7)−H(72)···O(200) #f	0.95(7)	1.79(8)	2.724(8)	166
O(100)−H(101)···O(8) #d	0.85(7)	2.25(6)	3.016(6)	150
O(100)−H(102)···O(200)	0.85(8)	2.17(10)	2.906(8)	146
		$[Co_2(C_8H_5NO_4)_2(C_4H_4N_2)]$ (**Ia**)		
N(2)−H(21)···O(5) #a	0.85(3)	2.20(3)	3.036(3)	169
N(2)−H(22)···O(8) #b	0.85(3)	2.25(3)	3.002(3)	148
N(4)−H(41)···O(2) #a	0.90	2.16	3.038(3)	166
N(4)−H(42)···O(7) #c	0.90	2.24	2.999(3)	142
		$[Ni_2(C_8H_5NO_4)_2(C_4H_4N_2)(H_2O)_2]\cdot 3H_2O$ (**II**)		
N(2)···H(21)···O(9) #a	0.83(6)	2.52(5)	3.202(6)	141
N(2)···H(22)···O(6) #b	0.95(6)	2.04(6)	2.932(5)	155
O(3)···H(31)···O(4) #c	0.95(4)	1.91(4)	2.855(5)	174
O(3)···H(32)···O(100) #d	0.94(5)	2.01(5)	2.917(7)	163
N(4)···H(41)···O(10) #e	0.88(6)	2.36(6)	3.109(5)	142
N(4)···H(42)···O(2) #b	0.83(6)	2.21(6)	2.946(5)	148
O(7)···H(72)···O(200) #f	0.95(5)	1.83(7)	2.735(7)	160
O(100)···H(101)···O(10) #e	0.85(5)	1.94(5)	2.775(6)	166
O(100)···H(102)···O(8) #d	0.85(5)	2.26(3)	3.111(6)	172
		$[Ni_2(C_8H_5NO_4)_2(C_4H_4N_2)]$ (**IIa**)		
N(2)−H(21)···O(6) #a	0.82(4)	2.15(5)	2.947(5)	165
N(2)−H(22)···O(9) #b	0.80(4)	2.43(4)	3.106(6)	144
N(4)−H(41)···O(2) #a	0.90	2.06	2.937(4)	163
N(4)−H(42)···O(10) #c	0.90	2.37	3.118(6)	140
		$[Co_2(H_2O)(\mu^3\text{-}OH)_2(C_8H_5NO_4)]$ (**III**)		
N(1)−H(51)···O(7) #a	0.86(8)	2.33(8)	3.123(10)	153
		$[Ni_2(H_2O)(\mu^3\text{-}OH)_2(C_8H_5NO_4)]$ (**IV**)		
O(1)−H(1)···O(3) #a	0.75(5)	2.54(5)	3.157(4)	141
N(1)−H(51)···O(7) #b	0.94(5)	2.21(5)	3.070(6)	153

[a] Symmetry transformations used to generate equivalent atoms. For **I**: #a 1−*x*,−1−*y*,2−*z*; #b 1−*x*,−*y*,1−*z*; #c 1−*x*,−*y*,2−*z*; #d 1−*x*,1−*y*,1−*z*; #e −*x*,−*y*,1−*z*; #f −1+*x*,*y*,*z*. For **Ia**: #a −*x*,2−*y*,−*z*; #b −*x*,1−*y*,1−*z*; #c 1−*x*,2−*y*,−*z*. For **II**: #a 1−*x*,−1−*y*,2−*z*; #b 1−*x*,−*y*,1−*z*; #c 1−*x*,−*y*,2−*z*; #d 1−*x*,1−*y*,1−*z*; #e −*x*,−*y*,1−*z*; #f −1+*x*,*y*,*z*; #g −*x*,1−*y*,1−*z*. For **IIa**: #a −*x*,2−*y*,−*z*; #b −*x*,1−*y*,1−*z*; #c 1−*x*,2−*y*,−*z*. For **III**: #a 1+*x*,*y*,*z*. For **IV**: #a 1+*x*,*y*,*z*; #b −*x*,−1/2+*y*,1/2−*z*.

(**II**) have been observed. The N−H···O interactions appear to be relatively weak. The important hydrogen bond interactions are given in Table 4.

The 3^6 layer topology observed in $[Co_2(C_8H_5NO_4)_2(C_4H_4N_2)(H_2O)_2]\cdot 3H_2O$ (**I**) and $[Ni_2(C_8H_5NO_4)_2(C_4H_4N_2)(H_2O)_2]\cdot 3H_2O$ (**II**) has also been observed in other MOF structures.[19] From a classical inorganic structural point of view, the 3^6 topology typically represents the $CdCl_2$ structure. A careful examination of the $CdCl_2$ structure (Figure 2a) and the present structure (Figure 2b) (metal ion and the AIP units are represented as spheres and arranged in a 2D lattice) clearly reveals close structural relationship between them (Figure 2). In the present compounds, the pyrazine unit connects the alternate adjacent layers, which gives rise to a bilayer structure. The metal centers in **I** and **II** are connected with only three AIP ligands instead of six, as expected for a $CdCl_2$ related structure arrangement. Thus, the present structures can be considered as an anion-deficient $CdCl_2$ [vertex sybol is $(4^6.6^6.8^3)(4^3)_2$] structure. The TOPOS[20] analysis for the whole bilayer structure reveals the vertex symbol for the AIP ligand as [6.6.6], for the binodal pyrazine as [8.(4)], and for both M(1) and M(2) it is $[6.8.6.8.6.8_2]$. The Schlafli symbol for the whole structure is $\{6^3;8^3\}_2\{6^3\}_2\{8\}$ (Supporting Information, Figure S7).

Structure of $[M_2(H_2O)(\mu^3\text{-}OH)_2(C_8H_5NO_4)]$, M = Co^{2+} (III) and Ni^{2+} (IV). The asymmetric unit of $[M_2(H_2O)(\mu^3\text{-}OH)_2(C_8H_5NO_4)]$, M = Co^{2+} (**III**) and Ni^{2+} (**IV**) consists of 18 non-hydrogen atoms, of which two M^{2+} ions are crystallographically independent along with one AIP anion, two μ^3-hydroxyl groups, and one coordinated water molecule. The independent M^{2+} ions have distorted octahedral coordination: M(1) is coordinated

(19) (a) Williams, C. A.; Blake, A. J.; Hubberstey, P.; Schröder, M. *Chem. Commun*. **2005**, 5435. (b) Kim, H.; Park, G.; Kim, K. *CrystEngComm*. **2008**, *10*, 954.

(20) (a) Blatov, V. A. **2006**, http://www.topos.ssu.samara.ru/. (b) Blatov, V. A.; Shevchenko, A. P.; Serezhkin, V. N. *J. Appl. Crystallogr*. **2000**, *33*, 1193.

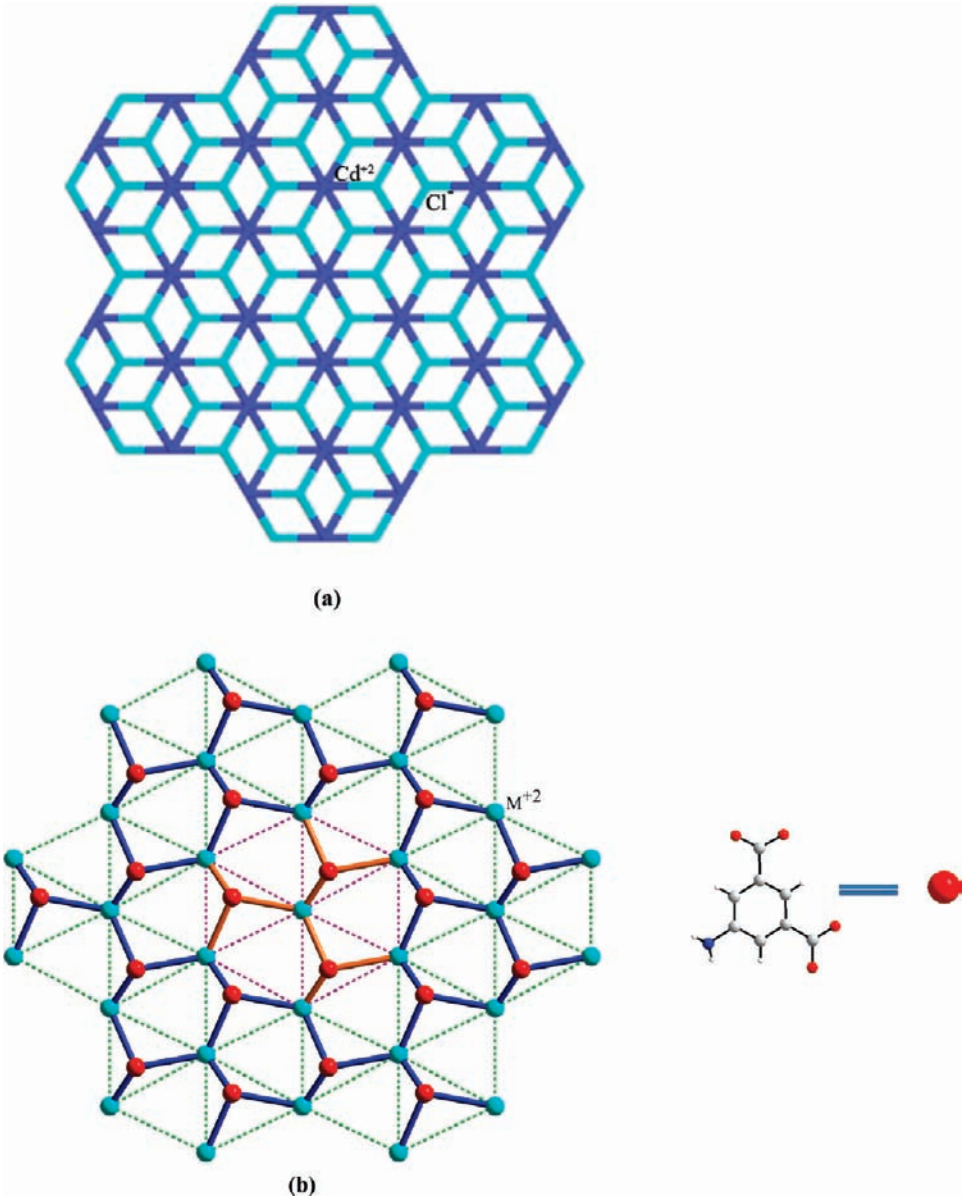

Figure 2. (a) View of the $CdCl_2$ structure. Color code for atoms: Cd, blue; Cl, cyan. (b) Connectivity between the metal center (green sphere) and the AIP unit (purple sphere). The dotted lines are a guide to the eye to bring out the close similarity between the structure of $[Co_2(C_8H_5NO_4)_2(C_4H_4N_2)(H_2O)_2]\cdot 3H_2O$ (**I**) and $[Ni_2(C_8H_5NO_4)_2(C_4H_4N_2)(H_2O)_2]\cdot 3H_2O$ (**II**) and $CdCl_2$. **I** and **II** and $CdCl_2$ structure (see text).

by four μ^3-hydroxyl ions and two carboxylate oxygen atoms forming MO_6 octahedra, and M(2) is coordinated by two μ^3-hydroxyl ions, two carboxylate oxygen, one aqua oxygen, and one nitrogen from the AIP ligand to form octahedral $MO_4(H_2O)N$. The M−O bond distances are in the range of 2.039(3)−2.358(6) Å (av. 2.114 Å) for Co, 2.022(3)−2.247(4) Å (av. 2.075 Å) for Ni; the M−N bond distance is 2.212(3) Å for Co, 2.150(4) Å for Ni. The O/N−M−O/N bond angles are in the range of 75.37(17)−174.58(11)° for Co and 78.11(14)−176.02(14)° for Ni. The selected bond distances are given in Table 3.

The structure of $[Co_2(H_2O)(\mu^3\text{-}OH)_2(C_8H_5NO_4)]$ (**III**) and $[Ni_2(H_2O)(\mu^3\text{-}OH)_2(C_8H_5NO_4)]$ (**IV**) can be understood by considering the connectivity between the metal centers. Thus, the octahedral metal centers are connected together through μ^3-hydroxyl groups (edgewise) to form a highly distorted one-dimensional −M−O(H)−M− chains (Figures 3a and S8). The chains are connected by the AIP units to form the three-dimensional structure, as shown in Figure 3b,c. Similar to the previous structures (**I** and **II**), the bonding of the amino group with the metal centers gives rise to N−H···O type hydrogen bonds (Table 4). A topological analysis of the structures **III** and **IV** gives an overall Schlafli symbol for the whole structure of $\{4^3;6\}\{4^3\}\{4^5;6^5\}\{4^6;6^4\}\{4^7;6^6;8^2\}$ (see Supporting Information, Figure S9).

Thermogravimetric Studies. Thermogravimetric analysis (TGA) on all compounds (**I** −**IV**) has been carried out in flowing air (flow rate = 20 mL min^{-1}) in the temperature range of 30−800 °C (heating rate = 5 °C min^{-1}) (see Supporting Information, Figure S10). The TGA studies indicate that compound $[Co_2(C_8H_5NO_4)_2(C_4H_4N_2)(H_2O)_2]\cdot 3H_2O$ (**I**) shows an initial weight loss of ~14.5% up to 180 °C, which may be due to the loss of the lattice and

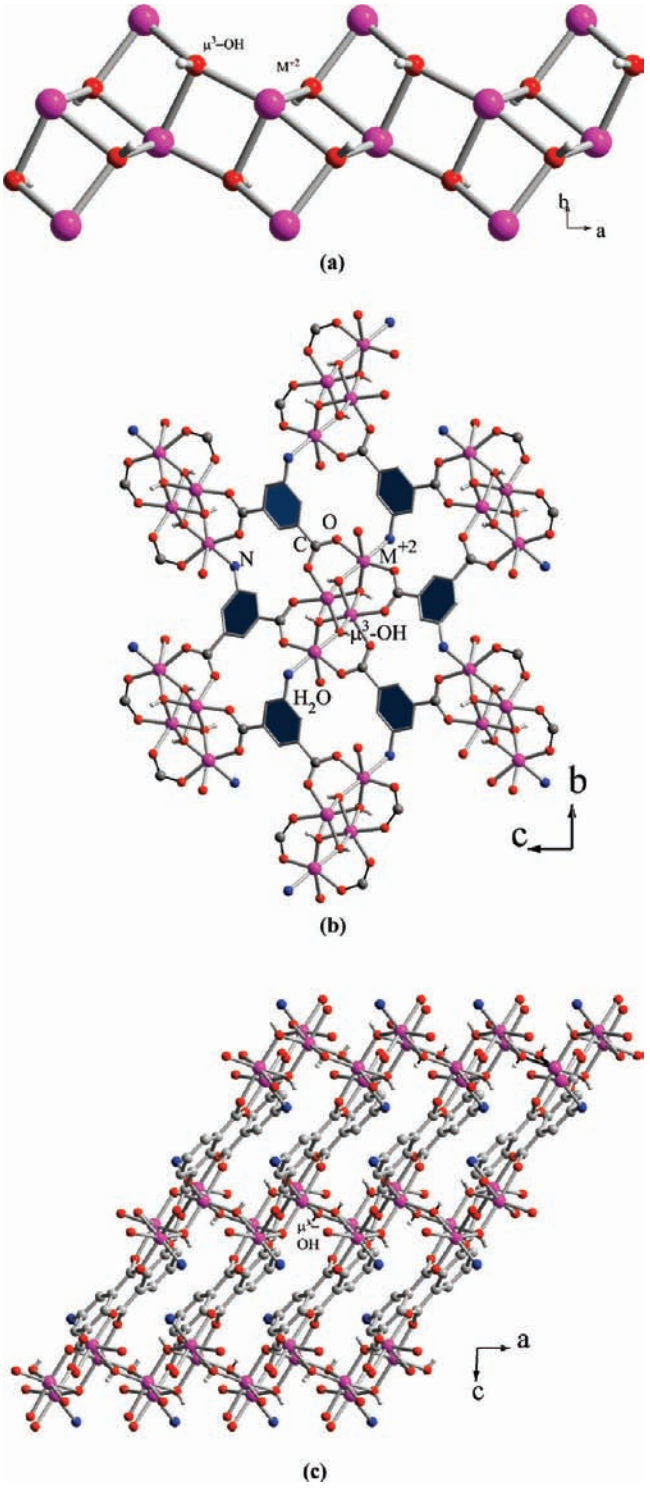

Figure 3. (a) View of the one-dimensional infinite −M−O(H)−M− chains observed in compounds $[Co_2(H_2O)(\mu^3\text{-}OH)_2(C_8H_5NO_4)]$ (**III**) and $[Ni_2(H_2O)(\mu^3\text{-}OH)_2(C_8H_5NO_4)]$ (**IV**). (b) Connectivity of aminoisophthalate with −M−O(H)−M− chains. (c) View of the three-dimensional structures of **III** and **IV**.

the coordinated water molecules, and the second weight loss of 62% at ∼315 °C corresponds to the carboxylate moieties. The total weight loss of 76.5% compares well with the loss of all the water molecules (coordinated and free) and the carboxylate units (calcd 74.5%). Compound $[Ni_2(C_8H_5NO_4)_2(C_4H_4N_2)(H_2O)_2]\cdot 3H_2O$ (**II**) also exhibits similar behavior with losses of 13% up to 180 °C and 66.1% at ∼335 °C. The total observed weight loss of 79.1% corresponds well with the loss of the carboxylate and all the water molecules (calcd 77%). Compound $[Co_2(H_2O)(\mu^3\text{-}OH)_2(C_8H_5NO_4)]$ (**III**) exhibits an initial weight loss of 7.5% at ∼140 °C and a second weight loss of 41% in the range of 290−310 °C. Compound $[Ni_2(H_2O)(\mu^3\text{-}OH)_2(C_8H_5NO_4)]$ (**IV**), on the other hand, appears to have a single step weight loss in the temperature range of 300−360 °C, which corresponds to loss of the coordinated water molecule along with all the carboxylate moieties. The total observed weight loss corresponds well with the loss in both cases of the carboxylate and water molecules of 48.5% (calcd 46%) and 53% (calcd 57%), respectively, for **III** and **IV** (see Supporting Information, Figure S10). The final calcined product in all cases was found to be crystalline by powder XRD and compounds to NiO (JCPDS: 73-1523) for the Ni-containing compound and to Co_3O_4 (JCPDS: 78-1970) for the Co-containing compounds.

UV−Visible Spectroscopic Studies. The diffuse reflectance UV−vis spectra at room temperature were recorded for the AIP anion (Na salt of AIP), pyrazine, and also for the as-synthesized compounds (see Supporting Information, Figure S11a and S11b). The NaAIP exhibited two main absorption peaks at ∼290 and 333 nm, whereas the pyrazine ligand has two main peaks at ∼252 and ∼315 nm. All of these peaks are due to the intraligand charge transfer transitions and appear as a broad peak in all compounds. In addition, we observed two additional peaks at 535 and 726 nm for $[Co_2(C_8H_5NO_4)_2(C_4H_4N_2)(H_2O)_2]\cdot 3H_2O$ (**I**), which may be due to the d−d transition of the d^7 (Co^{2+}) ion, and assigned to the $^4T_1g \rightarrow {}^4T_1g(P)$ and $^4T_1g \rightarrow {}^4A_2g(F)$ transitions.[21] Similarly characteristic d−d transitions have also been observed for other compounds, which are presented in Table 5.

Room temperature solid-state photoluminescence studies were carried out on the powdered samples (Perkin-Elmer, U.K. model no. LS55) (see Supporting Information, Figure S12a,b). All of the compounds, the AIP anion (Na salt of AIP), and the pyrazine ligand were excited at 260 nm. The emission bands were observed at ∼465 nm for Na-AIP and at ∼360, ∼422, and ∼490 nm for the pyrazine ligand. The emission bands can be assigned to the intraligand fluorescence. In addition, we also observed the emission bands due to the d−d transitions in all compounds. Thus, the emission bands at 545 and 731 nm for $[Co_2(C_8H_5NO_4)_2(C_4H_4N_2)(H_2O)_2]\cdot 3H_2O$ (**I**) can be assigned to the electronic transitions corresponding to $^4T_1g \rightarrow {}^4T_1g$ (P) and $^4T_1g \rightarrow {}^4A_2g$ transitions for the octahedral Co^{2+} ion.[22] The observed emission bands for all compounds are listed in Table 5.

In Situ Single Crystal to Single Crystal Transformation Studies. Structurally, compounds $[Co_2(C_8H_5NO_4)_2(C_4H_4N_2)(H_2O)_2]\cdot 3H_2O$ (**I**) and $[Ni_2(C_8H_5NO_4)_2(C_4H_4N_2)(H_2O)_2]\cdot 3H_2O$ (**II**) contain one terminal water molecule bonded with each metal ion, in addition to the lattice water molecules. Our TGA studies clearly indicated that the water molecules are removed below 200 °C.

(21) Lever, A. B. P. *Inorganic Electronic Spectroscopy*; Elsevier: NewYork, 1968.
(22) Blasse, G.; Grabmaier, B. C. *Luminescent Materials*; Springer-Verlag: Heidelberg, Germany, 1994.

Table 5. Observed UV−Visible Bands for Compounds **I**−**IV**[a]

no.	compound	UV−visible absorption bands (nm)		
		intraligand charge transfer	$^4T_1g \rightarrow {}^4T_1g(P)$	$^4T_1g \rightarrow {}^4A_2g(F)$
1	$[Co_2(C_8H_5NO_4)_2(C_4H_4N_2)(H_2O)_2]\cdot 3H_2O$ (**I**)	∼252 (P), ∼332(P), ∼382 (AIP)	∼525	∼726
2	$[Co_2(H_2O)(\mu^3\text{-}OH)_2(C_8H_5NO_4)]$ (**III**)	∼318 (A)	∼526	∼730
		intraligand charge transfer	$^3A_2g \rightarrow {}^3T_1g(P)$	$^3A_2g \rightarrow {}^3T_1g(F)$
3	$[Ni_2(C_8H_5NO_4)_2(C_4H_4N_2)(H_2O)_2]\cdot 3H_2O$ (**II**)	∼255(P), ∼315(P + A), ∼378(A)	∼405	∼665
4	$[Ni_2(H_2O)(\mu^3\text{-}OH)_2(C_8H_5NO_4)]$ (**IV**)	∼330(A), ∼380(A)	∼424	∼720
		UV−visible emission bands (in nm)		
		intraligand charge transfer	$^4T_1g \rightarrow {}^4T_1g(P)$	$^4T_1g \rightarrow {}^4A_2g(F)$
5	$[Co_2(C_8H_5NO_4)_2(C_4H_4N_2)(H_2O)_2]\cdot 3H_2O$ (**I**)	∼367(P), ∼448(P + A), ∼485(P)	∼535	∼725
6	$[Co_2(H_2O)(\mu^3\text{-}OH)_2(C_8H_5NO_4)]$ (**III**)	∼367(A), ∼420(A), ∼485(A)	∼532	∼727
		intraligand charge transfer	$^3A_2g \rightarrow {}^3T_1g(P)$	$^3A_2g \rightarrow {}^3T_1g(F)$
7	$[Ni_2(C_8H_5NO_4)_2(C_4H_4N_2)(H_2O)_2]\cdot 3H_2O$ (**II**)	∼448 (A), ∼487(P)	∼532	–
8	$[Ni_2(H_2O)(\mu^3\text{-}OH)_2(C_8H_5NO_4)]$ (**IV**)	∼368(A), ∼438(A), ∼487(A)	∼532	∼727

[a] A = AIP and P = pyrazine.

We wanted to investigate the dehydrated phase more closely to understand the stability as well as to determine its structure. Studies involving solvent removal, solvent exchange, and other related behavior of MOFs have been investigated via single crystal−single crystal transformations.[23] It has been shown that there could also be dimensionality changes during the dehydration process.[24] As part of this study, we have carried out the in situ single crystal−single crystal transformations involving the removal of the coordinated solvent of the synthesized MOFs. For this, a suitable single crystal was taken in a 0.3 mm capillary and mounted on the goniometer. The room temperature data were collected initially and checked for accuracy with the earlier data. The sample was heated using a flow of N_2 (heating rate = 40 K/h) to 125 °C (398 K). This temperature is marginally lower than the temperature observed for the release of the water molecules in our TGA studies (Figure S10). The temperature was maintained constant within an accuracy of 0.1 K. The data were collected and analyzed as described before.

Structure of $[M_2(C_8H_5NO_4)_2(C_4H_4N_2)]$, M = Co^{2+} (Ia) and Ni^{2+} (IIa). The dehydrated compounds $[Co_2(C_8H_5NO_4)_2(C_4H_4N_2)]$ (**Ia**) and $[Ni_2(C_8H_5NO_4)_2(C_4H_4N_2)]$ (**IIa**) are also isostructural but undergo a crystal system transformation from parent triclinic (**I** and **II**) to monoclinic (**Ia** and **IIa**). The asymmetric unit consists of 17 non-hydrogen atoms. The metal ions are coordinated by three carboxylate oxygens, one nitrogen from the amino group of the AIP anion, and one nitrogen from the pyrazine units forming a distorted square pyramidal environment (MO_3N_2, CN = 5). The change in the coordination around the central metal ions is also reflected in the bond distances as we observed a general shortening of the distances. The M−O bonds have distances in the range of 1.939(2)−2.348(2) Å for Co (av. 2.098 Å) and 1.952(3)−2.119(3) Å for Ni (av. 2.049 Å); the M−N bond distances are 2.085(2) and 2.094(2) Å for Co (av. 2.090 Å) and 2.046(4) and 2.057(3) Å for Ni (av. 2.052 Å). The O/N−M−O/N bond angles are in the range of 59.60(6)−159.15(7)° for Co and 62.46(10)−156.88(12)° for Ni. The selected bond distances are listed in Table 3. The compounds also retain the structural integrity of the parent phase as there is very little change in the bilayer arrangement described earlier. The structures of the fully dehydrated compounds are shown in Figure 4a,b. The loss of the water molecules from the structure leads to the complete loss of all O−H···O hydrogen bonds from the parent structure. The N−H···O hydrogen bonds, however, are present and did not exhibit any marked change (Table 4).

The asymmetric unit of $[Co_2(C_8H_5NO_4)_2(C_4H_4N_2)(H_2O)_2]\cdot 3H_2O$ (**I**) and $[Ni_2(C_8H_5NO_4)_2(C_4H_4N_2)(H_2O)_2]\cdot 3H_2O$ (**II**) has two distinct M^{2+} ions, both of which has a coordinated water molecule. We desired to investigate the release of the coordinated water molecule as a function of temperature to examine whether the coordinated and the lattice water molecules are removed simultaneously or at different temperatures. For this, a suitable single crystal of compound **I** was loaded in a capillary and heated slowly. At 80 °C, we observed that one of the M^{2+} ions lost the coordinated water molecule (becomes distorted square pyramidal), while the other M^{2+} ion continues to be in the octahedral environment (compounds $[Co_2(C_8H_5NO_4)_2(C_4H_4N_2)(H_2O)]\cdot H_2O$ (**Ib**) and $[Ni_2(C_8H_5NO_4)_2(C_4H_4N_2)(H_2O)]\cdot H_2O$ (**IIb**); see Figure S13). The other M^{2+} ion eventually lost the bonded water molecules when heated to 125 °C as described before. We did not observe any drastic changes in the bonding between the M^{2+} and its nearest neighbors. The present study clearly demonstrates

(23) (a) Xiao, Bo.; Byrne, P. J.; Wheatley, P. S.; Wragg, D. S.; Zhao, X.; Fletcher, A. J.; Thomas, K. M.; Peters, L.; Evans, J. S. O.; Warren, J. E.; Zhou, W.; Morris, R. E. *Nat. Chem.* **2009**, *1*, 289. (b) Bernini, M. C.; Gandara, F.; Iglesias, M.; Snejko, N.; Gutierrez-Puebla, E.; Brusau, E. V.; Narda, G. E.; Monge, M. A. *Chem.—Eur. J.* **2009**, *15*, 4896. (c) Lee, J. Y.; Lee, S. Y.; Sim, W.; Park, K.; Kim, J.; Lee, S. S. *J. Am. Chem. Soc.* **2008**, *130*, 6902. (d) Ghosh, S. K.; Zhang, J. P.; Kitagawa, S. *Angew. Chem., Int. Ed.* **2007**, *46*, 7965. (e) Chen, C. L.; Goforth, A. M.; Smith, M. D.; Su, C. Y.; Loye, H. C. *Angew. Chem., Int. Ed.* **2005**, *44*, 6673. (f) Lee, E. Y.; Suh, M. P. *Angew. Chem., Int. Ed.* **2004**, *43*, 2798.

(24) (a) Zhang, Y. J.; Liu, T.; Kanegawa, S.; Sato, O. *J. Am. Chem. Soc.* **2009**, *131*, 7942. (b) Cheng, X. N.; Zhang, W. X.; Chen, X. M. *J. Am. Chem. Soc.* **2007**, *129*, 15738. (c) Chu, Q.; Swenson, D. C.; MacGillivray, L. R. *Angew. Chem., Int. Ed.* **2005**, *44*, 3569.

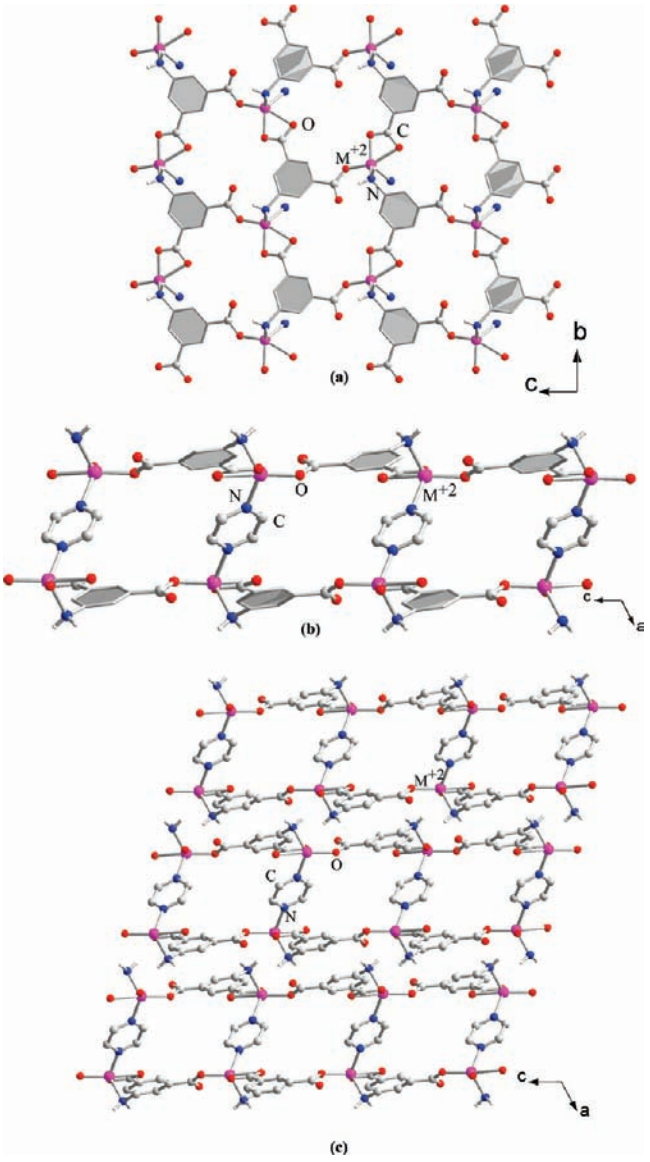

Figure 4. (a) View of the layer in the fully dehydrated compounds $[Co_2(C_8H_5NO_4)_2(C_4H_4N_2)]$ (**Ia**) and $[Ni_2(C_8H_5NO_4)_2(C_4H_4N_2)]$ (**IIa**). (b) Connectivity between the layers via pyrazine in **Ia** and **IIa**. (c) Bilayer arrangement in **Ia** and **IIa**. (Note the close similarity between **I** and **Ia** and **II** and **IIa**.)

the release of water is not a simple single-step process but a slow two-step process. This was also confirmed by our DSC studies, which clearly exhibited two steps at ~80 and ~125 °C (Figure S15a). The steps observed at lower temperatures in the DSC correspond to the loss of the lattice water molecules (free), and the second peak corresponds to the removal of the two coordinated water molecule from the structure. The calculated molar enthalpy for the second peak is 15.72 kcal mol^{-1}, which would correspond to 7.86 kcal mol^{-1} for the released one-bonded water molecule. Now, the change in geometry of a Co^{2+} ion from octahedral to a distorted square pyramidal geometry gives a crystal field stabilization energy equivalent to −1.14 dq [(−9.14 dq)−(−8dq)], which would be the main contributor for this gain in the molar enthalpy of 7.86 kcal.

Since the compound loses the bonded water molecules at 125 °C, we wanted to investigate whether the water molecules can be replaced by D_2O. For this, the dehydrated crystals of $[Co_2(C_8H_5NO_4)_2(C_4H_4N_2)(H_2O)_2]\cdot 3H_2O$ (**I**) were left to soak in D_2O at room temperature. The IR study of the samples shows that the D_2O molecule replaces the water molecules in the structures. Our efforts to introduce other guest species, such as methanol, acetonitrile, etc., were not successful. It is likely that the available spaces within the double layer may not be sufficient to incorporate these molecules. The summary of the single crystal to single crystal transformation is presented in Figure 5.

Dynamics of the Water Molecules. (a). Thermal Studies. The TGA studies of compounds $[Co_2(C_8H_5NO_4)_2(C_4H_4N_2)(H_2O)_2]\cdot 3H_2O$ (**I**) and $[Ni_2(C_8H_5NO_4)_2(C_4H_4N_2)(H_2O)_2]\cdot 3H_2O$ (**II**) reveal that the water molecules are lost below ~200 °C, which prompted us to examine the possible reversible adsorption of the water molecules. Our single crystal−single crystal transformation studies also indicated that the dehydrated sample rehydrates quickly on cooling to room temperature (we observed identical structure). The reversibility of water adsorption was carried out in a modified TGA setup containing a port for introducing the water vapor. The sample was taken in the TGA crucible and heated to the temperature of complete dehydration[25] in an atmosphere of flowing dry nitrogen (50 mL/min) (180 °C for both **I** and **II**) using a heating rate of 5 °C/min. The samples were cooled slowly to room temperature (cooling rate = 2 °C/min), and saturated water vapor was introduced into the system for rehydration for 60 min. During this process, we observed that both samples reabsorbed the water molecules and reached the original weights. Thus, 99.3 and 92.8% of the initial weight was absorbed from the dehydrated weights of 87 and 84% for **I** and **II**, respectively. Both compounds reabsorbed fully if kept for longer duration in the open environment. Though this behavior was expected, our purpose was to examine the recyclability of the dehydration−rehydration behavior. So dehydration and rehydration experiment was repeated consequently four times, resulting in identical behavior for both compounds **I** and **II** (Figures 6 and S14). This observation confirms that the dehydration−rehydration behavior is fully reversible. The powder XRD pattern recorded on the fully rehydrated sample also confirms that the integrity of the samples are retained.

(b). Temperature-Programmed In Situ IR Spectroscopic Studies. To understand the possible reversible hydration behavior of compounds $[Co_2(C_8H_5NO_4)_2(C_4H_4N_2)(H_2O)_2]\cdot 3H_2O$ (**I**) and $[Ni_2(C_8H_5NO_4)_2(C_4H_4N_2)(H_2O)_2]\cdot 3H_2O$ (**II**), we further carried out in situ diffuse reflectance IR spectroscopic (DRIFTS) studies (Perkin-Elmer, SPECTRUM-2000, MCT detector) in the range from 25 to 170 °C as the IR is quite sensitive for the water molecules. The coordinated and lattice water bands appear at 3401 and 3530 cm^{-1} for compound **I** and 3482 and 3539 cm^{-1} for compound **II** (Figures 8a and S16a, respectively). The changes to this water bands were monitored as a function of temperature. As can be noted, the bands gradually disappear with increasing

(25) Chandler, B. D.; Cramb, D. T.; Shimizu, G. K. H. *J. Am. Chem. Soc.* **2006**, *128*, 10403.

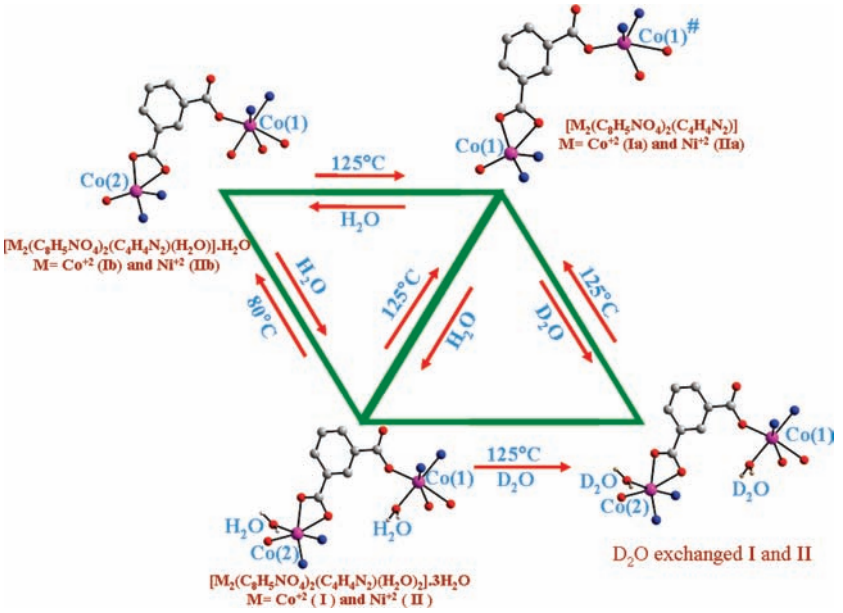

Figure 5. (a) Schematic summarizing the dehydration−rehydration studies of $[Co_2(C_8H_5NO_4)_2(C_4H_4N_2)(H_2O)_2]\cdot 3H_2O$ (**I**) and $[Ni_2(C_8H_5NO_4)_2(C_4H_4N_2)(H_2O)_2]\cdot 3H_2O$ (**II**).

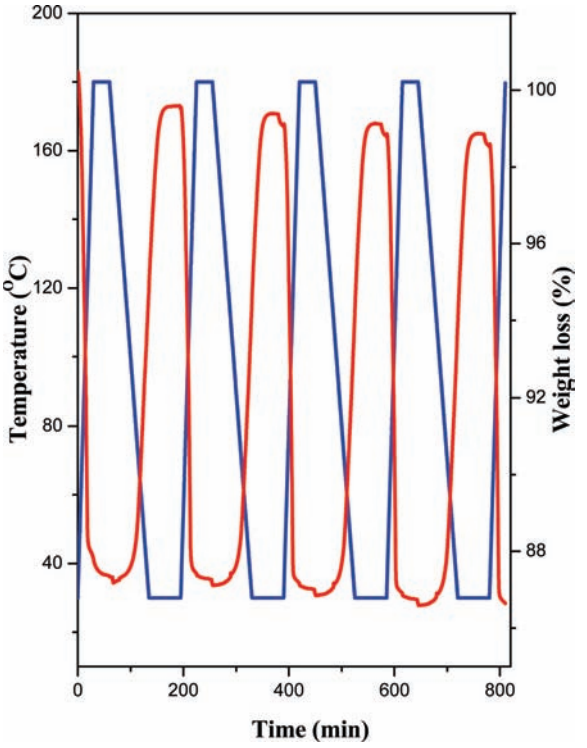

Figure 6. Reversible water uptake study of compound $[Co_2(C_8H_5NO_4)_2(C_4H_4N_2)(H_2O)_2]\cdot 3H_2O$ (**I**) using TGA. The blue curve represents the heating and cooling cycle, and the red curve represents the weight loss and weight gain.

temperature, confirming the removal of both the coordinated and the lattice water molecules from the structures. To investigate the reversible uptake of H_2O, we made efforts to replace the water molecules with D_2O and study the dehydration behavior. For this purpose, the fully dehydrated sample was taken at 125 °C in a closed vessel. The D_2O exchanged samples were subjected to a similar study using DRIFTS. The IR spectra of the deuterated sample indicated bands at 2575 and 2535 cm^{-1} for compound **I** and 2484 and 2440 cm^{-1} for compound **II** (Figures 8b and S16b, respectively), which corresponds to the coordinated and lattice D_2O stretching vibration.[26] As can be seen, we did not observe any peaks corresponding to the water, suggesting that both the coordinated and the lattice water molecules were completely replaced by D_2O. The DRIFTS studies on the deuterated samples also exhibited a behavior similar to the as-prepared sample when heated under identical conditions. Thus, the D_2O stretching band also loses the intensity with increasing temperature and finally disappears. This study clearly establishes the complete reversibility of the water molecules in both compounds **I** and **II**.

(c). Optical Studies. The reversibility of the water adsorption and the change in the coordination environment can be visualized by the change in color of the compounds (Figure 7a,b). Compound $[Co_2(C_8H_5NO_4)_2(C_4H_4N_2)(H_2O)_2]\cdot 3H_2O$ (**I**) changes from purple to blue, and compound $[Ni_2(C_8H_5NO_4)_2(C_4H_4N_2)(H_2O)_2]\cdot 3H_2O$ (**II**) changes from light greenish to brown after dehydration. The dehydrated samples return to the original color within a few minutes of exposure to the atmospheric conditions. This change of color can be attributed to the change of the crystal field splitting of the central M^{2+} ions, which changes from the octahedral coordination to the distorted square pyramidal coordination during the removal of the bonded water molecules.

The change of the color of the Co and Ni compounds upon dehydration prompted us to study the changes in the electronic transitions in the dehydrated sample. For this, the compounds were heated under vacuum in a glass tube for 2 h at 180 °C, and the resulting blue (**I**) and brown (**II**) colored samples were carefully transferred to a quartz sealed cuvette under inert conditions (glovebox). The UV−vis spectra of the dehydrated sample were recorded at room temperature. The UV−vis spectra of the

(26) Nakamoto, K. *Infrared and Raman Spectra of Inorganic and Coordination Compounds*; Wiley-Interscience: New York, 1963.

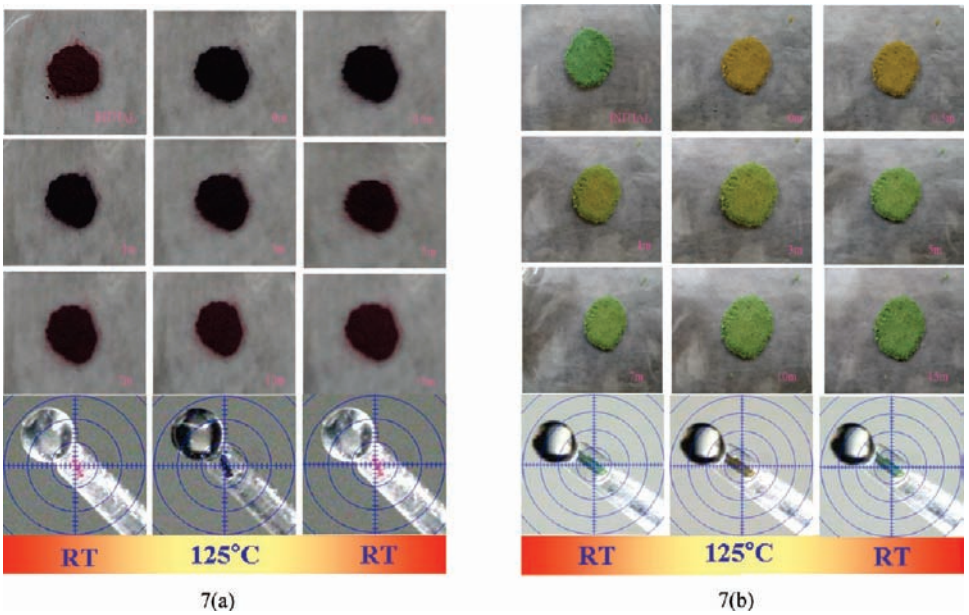

Figure 7. Change in color during dehydration and rehydration in the bulk as well as single crystals for (a) compound $[Co_2(C_8H_5NO_4)_2(C_4H_4N_2)(H_2O)_2]\cdot 3H_2O$ (**I**) and (b) compound $[Ni_2(C_8H_5NO_4)_2(C_4H_4N_2)(H_2O)_2]\cdot 3H_2O$ (**II**).

dehydrated sample of $[Co_2(C_8H_5NO_4)_2(C_4H_4N_2)(H_2O)_2]\cdot 3H_2O$ (**I**) show absorption bands at 615 and 870 nm (Figure 9a). The absorption bands at ~615 nm could be due to the $^4A_2'(F) \rightarrow {}^4E''(P)$ transition, and the absorption band at ~870 could be due to the $^4A_2'(F) \rightarrow {}^4A_2'(P)$ transition of the square pyramidal d^7 (Co^{2+}) ion. Similarly, the dehydrated sample of compound $[Ni_2(C_8H_5NO_4)_2(C_4H_4N_2)(H_2O)_2]\cdot 3H_2O$ (**II**) exhibited absorption bands at 495 and 845 nm (Figure S17a). The absorption bands at ~495 nm could be due to the $^3E' \rightarrow {}^3E''$ transition, and the absorption bands at ~845 nm could be due to the $^3E' \rightarrow {}^3A_1'', {}^3A_1''$ transitions of the square pyramidal d^8 (Ni^{2+}) ion.

To investigate the rehydration behavior more clearly, the UV−vis spectra of the dehydrated samples were studied by exposing the sample to the atmospheric conditions. As can be noted, the intensity of the transitions corresponding to the dehydrated state starts to decrease slowly along with the increase in the intensity of the rehydrated state as a function of time (Figures 9b and S17b for **I** and **II**, respectively) . This observation also confirms the change in coordination during rehydration accompanying the change in the color.

Sorption Studies. The reversibility of the rehydration and dehydration of the framework structure with the retention of single crystallinity is important and interesting. We also sought to investigate the water sorption behavior of compounds $[Co_2(C_8H_5NO_4)_2(C_4H_4N_2)(H_2O)_2]\cdot 3H_2O$ (**I**) and $[Ni_2(C_8H_5NO_4)_2(C_4H_4N_2)(H_2O)_2]\cdot 3H_2O$ (**II**). For this, a preheated sample (180 °C) was used, and the water absorption isotherms were measured at 298 K. The compounds show a gradual uptake of water with a total of 166 mL/g (4.16 mol of H_2O/mol of **I**) and 101 mL/g (2.53 mol of H_2O/mol of **II**) for the compounds **I** and **II**, respectively, at $P/P_0 = 1$ (Figure 10). The uptake of water is consistent with our TGA data. The rapid uptake of water at very low pressure is a characteristic of a microporous solid, which can also be attributed to the unsaturated coordination around the metal centers. The compounds, however, do not show any considerable hysteresis in the desorption curve, which suggests that both the rehydration and the dehydration processes could be effected with ease.

Magnetic Studies. Temperature-dependent magnetic susceptibility measurements for all compounds have been performed on powdered samples using a SQUID magnetometer (Quantum Design Inc., USA). The observed magnetic moment for compound $[Co_2(C_8H_5NO_4)_2(C_4H_4N_2)(H_2O)_2]\cdot 3H_2O$ (**I**) at room temperature (300 K) is 4.56 μ_B, which is larger than the calculated spin-only value of 3.87 μ_B for Co^{2+}. This suggests a significant orbital contribution for compound **I**. The variation of the inverse of the susceptibility as a function of temperature was fitted to the Curie−Weiss behavior (50−300 K) to obtain a Curie constant $C = 2.78$ emu/mol and Weiss temperature $\theta_P = -41.8$ K. This indicates that the interactions between the Co^{2+} ions are antiferromagnetic. The observed magnetic moment for compound $[Ni_2(C_8H_5NO_4)_2(C_4H_4N_2)(H_2O)_2]\cdot 3H_2O$ (**II**) at 300 K was 2.56 μ_B, which corresponds to the moment for the noninteracting paramagnetic Ni^{2+} ions and agrees with the spin-only magnetic moment of the Ni^{2+} ion in the octahedral field (2.83 μ_B). The temperature variation of the inverse susceptibility fitted to Curie−Weiss law, in the temperature range of 50−300 K, gives a value of $C = 0.88$ emu/mol and a $\theta_P = 1.55$ K. The small positive θ_P indicates possible ferromagnetic correlations between the Ni^{2+} ions in **II** (see Supporting Information, Figure S18).

The presence of M−O(H)−M connectivity and short M−M distances in compounds $[Co_2(H_2O)(\mu^3\text{-}OH)_2(C_8H_5NO_4)]$ (**III**) and $[Ni_2(H_2O)(\mu^3\text{-}OH)_2(C_8H_5NO_4)]$ (**IV**) suggests a more interesting magnetic behavior in both the compounds. In the light of this, it may be noted that Monge and co-workers have also observed a long-range 3D magnetic ordering in $Co_2[O_8C_{10}H_2]$, which possess one-dimensional Co−O−Co chains.[27] At room temperature, the $\chi_M T$ value of **III** is 5.10 emu mol^{-1} K for

(27) Snejko, N.; Gutiérrez-Puebla, E.; Martínez, J. L.; Monge, M. A.; Ruiz-Valero, C. *Chem. Mater.* **2002**, *14*, 1879.

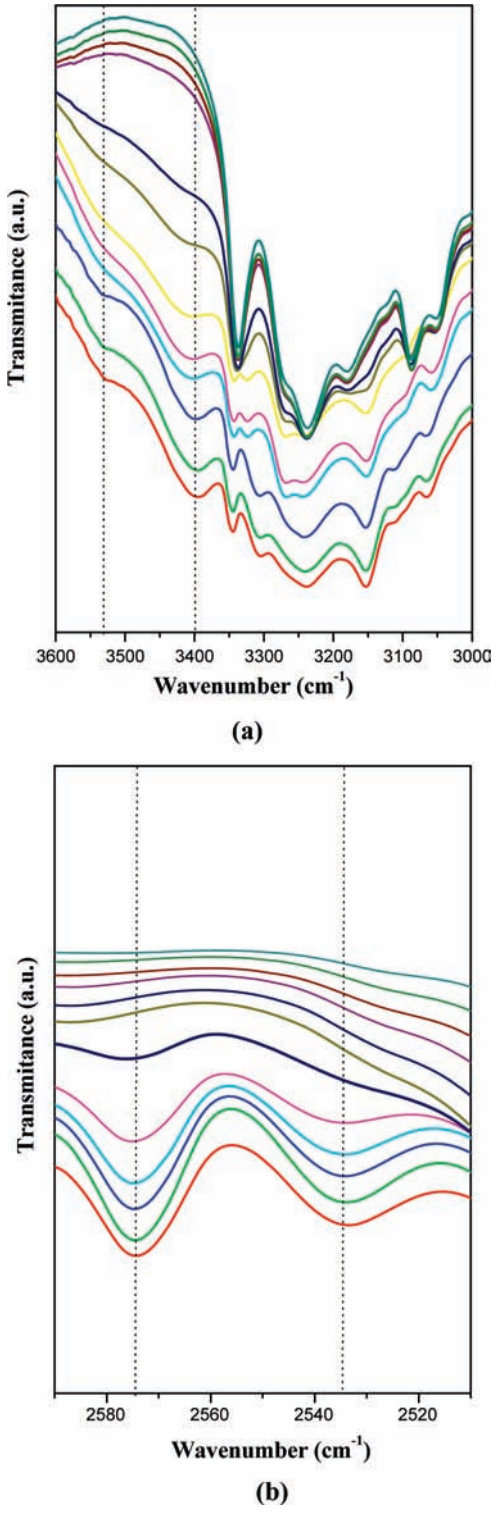

Figure 8. In situ diffuse reflectance IR spectra (DRIFTS) of compound $[Co_2(C_8H_5NO_4)_2(C_4H_4N_2)(H_2O)_2]\cdot 3H_2O$ (**I**) as a function of temperature showing the disappearance of the (a) H_2O bands at 3401 and 3530 cm^{-1} and (b) D_2O bands at 2535 and 2575 cm^{-1}. The dashed line is a guide to the eye.

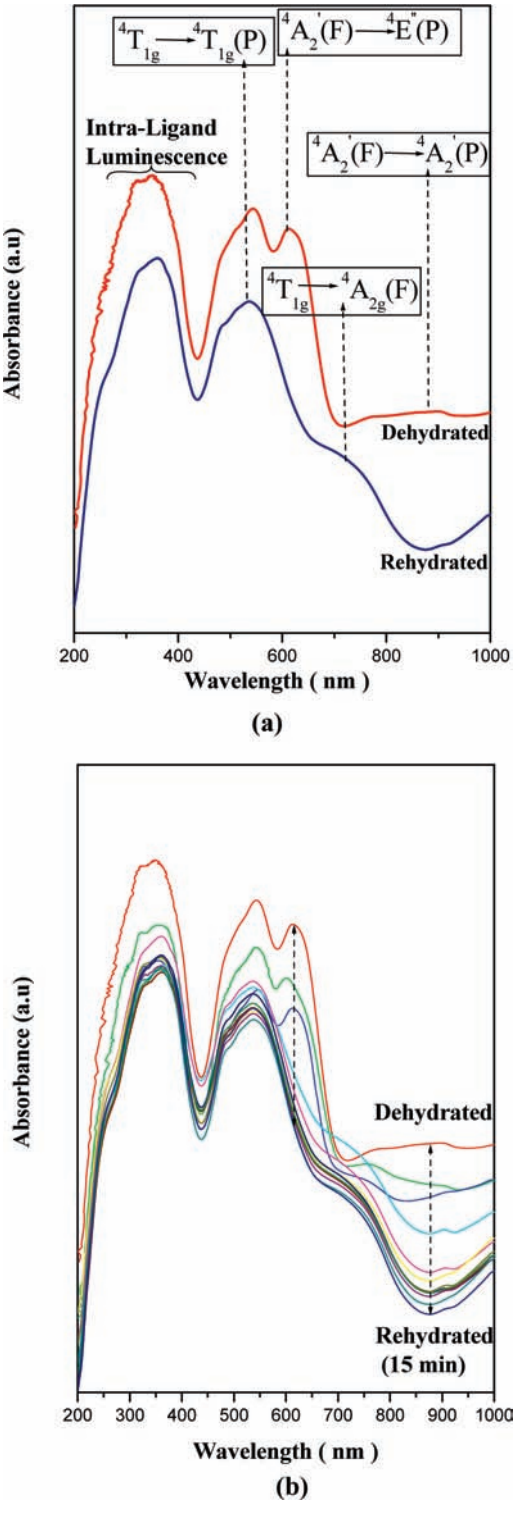

Figure 9. (a) UV−vis spectra of compound $[Co_2(C_8H_5NO_4)_2(C_4H_4N_2)(H_2O)_2]\cdot 3H_2O$ (**I**) (blue) and the dehydrated phase (red). (b) UV−vis spectra of the dehydrated sample after exposure to the atmosphere for various times (0−15 min).

two Co^{2+} ions, which is considerably higher than the spin-only value (3.75 emu mol^{-1} K) due to the orbital contribution. The χ_M values more or less remain unchanged for **III** when the sample was cooled and start to show an increase at low temperatures. The χ_M value increases sharply below 50 K and reaches a maximum at ~18 K, suggesting the onset of long-range magnetic ordering. The χ_M value starts to decrease upon cooling further to the lowest temperature of measurement (2 K). The $1/\chi_M$ versus T curve is shown as the inset of Figure 11a. The high-temperature magnetic data (150−300 K) were fitted to the Curie−Weiss behavior with $C = 2.99$ emu mol^{-1} and $\theta_P = -54.58$ K, indicative of antiferromagnetic

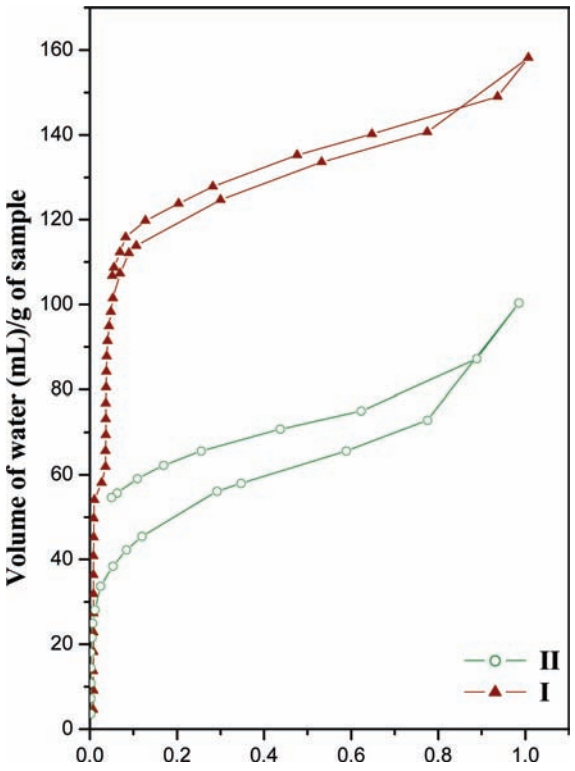

Figure 10. Water vapor adsorption−desorption isotherms for compounds $[Co_2(C_8H_5NO_4)_2(C_4H_4N_2)(H_2O)_2]\cdot 3H_2O$ (**I**) and $[Ni_2(C_8H_5NO_4)_2(C_4H_4N_2)(H_2O)_2]\cdot 3H_2O$ (**II**).

exchange between the Co^{2+} ions in **III**. The large Weiss constant along with the high ordering temperature suggests that the overlap between the Co^{2+} centers and the O(H) groups is strong and paves away for stronger superexchanged interactions. The field-cooled (FC) and zero-field-cooled (ZFC) magnetization data measured at 1000 Oe down to 2 K do not show any deviation (Figure 11a). The field-cooled $\chi_M T$ versus T curve at different applied dc fields clearly shows the onset of spontaneous magnetization below ∼50 K and shows the field-induced magnetizations up to 2500 Oe (Figure 11b). This suggests that the moments of the lattices rotate proportionally to the applied field up to about 2500 Oe, where it starts to saturate to a value approaching the expected moment per cobalt(II).[28] The $M(H)$ studies at 2 K show a hysteresis loop with a coercive field (H_c) of 383 Oe and remanance magnetization (M_r) of 0.68 μ_B (Figure 11c). The ac magnetic susceptibility studies also exhibit a sharp increase at ∼18 K, suggestive of the transition temperature (Figure S19).

The magnetic behavior of compound $[Co_2(H_2O)(\mu^3\text{-}OH)_2(C_8H_5NO_4)]$ (**IV**), on the other hand, indicates a different behavior. At room temperature, it has a $\chi_M T$ value of 2.86 emu mol^{-1} K for two Ni^{2+} ions, which is slightly higher than the spin-only value (2 emu mol^{-1} K) due to the orbital contribution. As can be noted, the χ_M values increase gradually upon cooling to reach a maximum at $T \sim 24$ K, indicative of the onset of long-range magnetic ordering. The χ_M value starts to decrease on cooling up to 5 K, beyond which it increases again. The $1/\chi_M$ versus T curve is shown as the inset of Figure 12a. The high-temperature magnetic susceptibility data (150−300 K) fitted to the Curie−Weiss behavior with $C = 1.60$ emu mol^{-1} and $\theta_P = -92.1$ K indicate that the dominant exchanges are predominantly antiferromagnetic. The large Weiss constant along with a reasonably high ordering temperature suggests a good overlap between the metal and the oxygen orbitals in **IV**. The field-cooled $\chi_M T$ versus T curve at different applied dc fields clearly shows the onset of spontaneous magnetization below 40 K, along with an increase in $\chi_M T$ values as the applied field decreases. This behavior is suggestive of a canted antiferromagnetic behavior (Figure 12b). The difference between the field-cooled (FC) and the zero-field-cooled (ZFC) susceptibility values at low temperatures indicates that there could be a ferromagnetic-like correlation[29] (Figure 12a). This is also confirmed by our $M(H)$ studies at 2 K, which shows a small hysteresis loop with a coercive field (H_c) of 1808 Oe and remanance magnetization (M_r) of 0.29 μ_B (Figure 12c). The canting angle of compound **III** is calculated to be ca. 8.25°, based on the equation $\psi = \tan^{-1}(M_r/M_s)$.[30] Also, the real and imaginary parts of the ac magnetic susceptibility exhibit a sharp increase at ∼21 K and show frequency-dependent maxima as a function of temperature (Figure S20), suggestive of the transition.

Though both $[Co_2(H_2O)(\mu^3\text{-}OH)_2(C_8H_5NO_4)]$ (**III**) and $[Ni_2(H_2O)(\mu^3\text{-}OH)_2(C_8H_5NO_4)]$ (**IV**) are isomorphous, they show rather different magnetic behavior. In the case of cobalt (**III**), we observe a field-induced magnetization, whereas the nickel compound (**IV**) shows canted antiferromagnetism. However, both of them show weak ferromagnetic interactions at low temperature. There are two mechanisms by which weak ferromagnetism may occur; it can be either single-ion anisotropy and/or antisymmetric spin−spin coupling.[31] It is to be noted that, for the two isomorphous systems, the isotropic exchange and the antisymmetric one should be of the same order, and therefore, the local anisotropy is the dominant factor which determines the magnetic behavior. The local anisotropy of the Co^{2+} ions is due to first-order spin−orbit coupling being, thus, greater than that for Ni^{2+}, which is due only to the second-order spin−orbit coupling. Therefore, Co^{2+} ions are, inherently, much more anisotropic than Ni^{2+} ions (for isomorphous complexes). Probably this greater local anisotropy of Co^{2+} results in the field-induced magnetization in **III**, whereas **IV** behaves as canted antiferromagnet. However, this magnetic difference in the two Co^{2+} and Ni^{2+} isomorphous complexes is still very rare in the literature.

Conclusion

The synthesis and structure of four new 5-aminoisophthalates (AIP) of cobalt and nickel have been accomplished.

(28) Kumagai, H.; Kepert, C. J.; Kurmoo, M. *Inorg. Chem.* **2002**, *41*, 3410.

(29) (a) Mahata, P.; Sen, D.; Natarajan, S. *Chem. Commun.* **2008**, 1278. (b) Mahata, P.; Sundaresan, A.; Natarajan, S. *Chem. Commun.* **2007**, 4471. (c) Yang, M.; Yu, J.; Shi, L.; Chen, P.; Li, G.; Chen, Y.; Xu, R.; Gao, S. *Chem. Mater.* **2006**, *18*, 476.

(30) Li, J. R.; Yu, Q.; Sanudo, E. C.; Tao, Y.; Bu, X. H. *Chem. Commun.* **2007**, 2602.

(31) Carlin, R. L. *Magnetochemistry*; Springer-Verlag: Berlin, 1986.

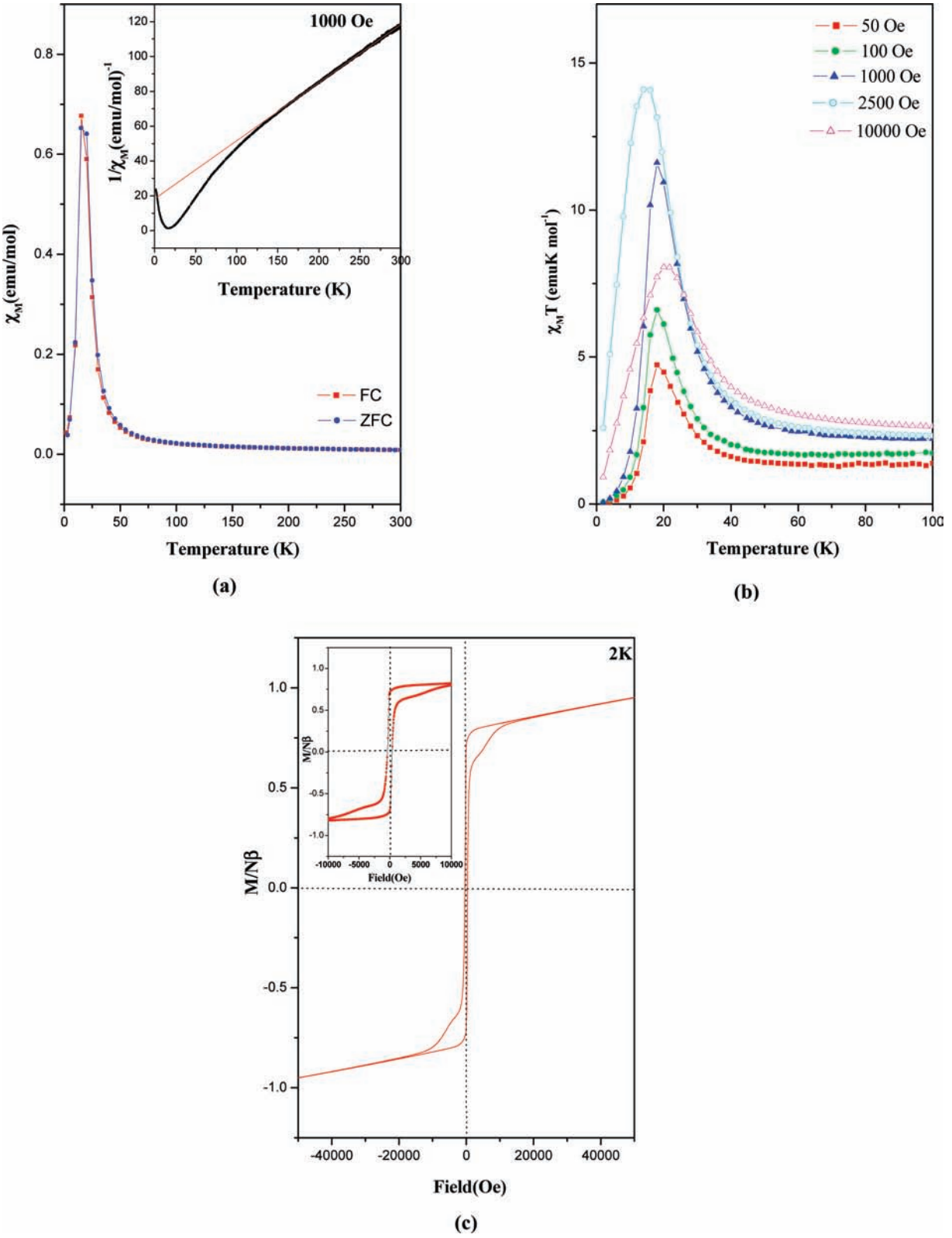

Figure 11. Magnetic behavior of compound $[Co_2(H_2O)(\mu^3\text{-}OH)_2(C_8H_5NO_4)]$, (**III**). (a) Field-cooled and zero-field-cooled (H = 1000 Oe). Inset shows the $1/\chi_M$ vs T plot. (b) Variation of $\chi_M T$ vs T plot as a function of applied dc field. (c) M vs H plot at 2 K. Inset shows enlarged view.

Compounds $[Co_2(C_8H_5NO_4)_2(C_4H_4N_2)(H_2O)_2]\cdot 3H_2O$ (**I**) and $[Ni_2(C_8H_5NO_4)_2(C_4H_4N_2)(H_2O)_2]\cdot 3H_2O$ (**II**) have a bilayer arrangement, wherein alternate anion-deficient $CdCl_2$ related layers are bridged by a pyrazine ligand. Compounds $[Co_2(H_2O)(\mu^3\text{-}OH)_2(C_8H_5NO_4)]$ (**III**) and $[Ni_2(H_2O)(\mu^3\text{-}OH)_2(C_8H_5NO_4)]$ (**IV**) have one-dimensional infinite M−O(H)−M chains bridged by AIP units. The coordinated and lattice water molecules in **I** and **II** are reversibly removed along with changes in color of the sample. The quick response of the dehydrated samples (**Ia** and **IIa**) for

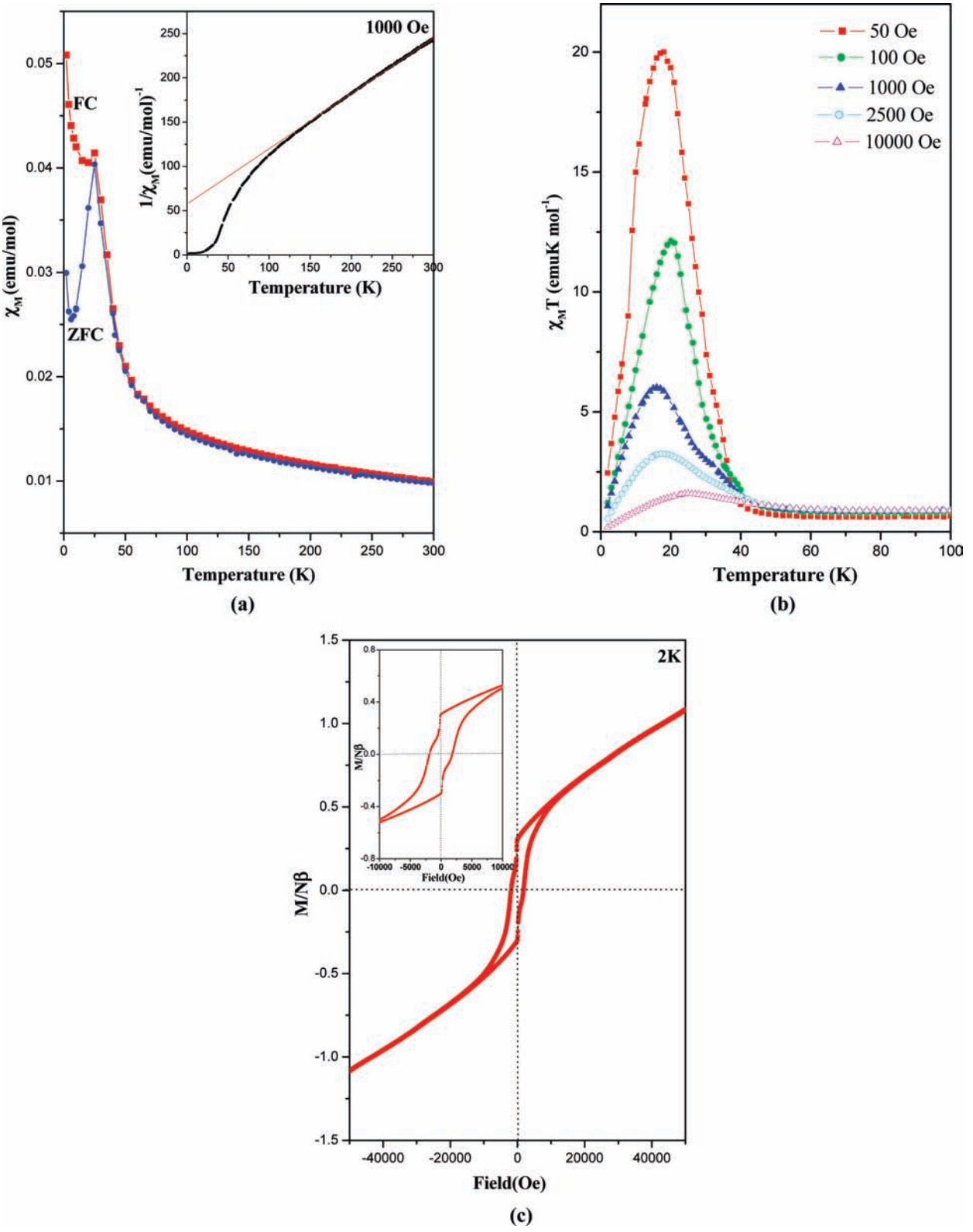

Figure 12. Magnetic behavior of compound $[Ni_2(H_2O)(\mu^3\text{-}OH)_2(C_8H_5NO_4)]$, (**IV**). (a) Field-cooled and zero-field-cooled plot of χ_M vs T at $H = 1000$ Oe. Inset shows the $1/\chi_M$ vs T plot. (b) $\chi_M T$ vs T plot at various dc fields. (c) M vs H plot at 2 K. Inset shows enlarged view.

water vapor (atmospheric conditions) suggests that these compounds could be exploited as possible water sensors. The magnetic studies on **III** show field-induced magnetization, whereas **IV** indicates a canted antiferromagnetic behavior. Because it is likely that the use of amino carboxylic acid would provide possible new types of framework structures with interesting properties, work toward this goal is in process.

Acknowledgment. S.N. thanks the Department of Science and Technology (DST), Government of India, for the award of a research grant, and the authors thanks

the Council of Scientific and Industrial Research (CSIR), Government of India, for the award of a fellowship (D.S.) and a research grant. S.N. also thanks the Department of Science and Technology, Government of India, for the award of the RAMANNA fellowship. K.V.R. acknowledges the receipt of CP-STIO grant from the Department of Science and Technology, Government of India. S.E.L. acknowledges support of NSF MRSEC Grant DMR 0520471.

Supporting Information Available: Additional experimental details and figures. This material is available free of charge via the Internet at http://pubs.acs.org.